A computational study of the binding of 3-(arylidene) anabaseines to two major brain nicotinic acetylcholine receptors and to the acetylcholine binding protein. Eur J Med Chem

ARTICLE *in* EUROPEAN JOURNAL OF MEDICINAL CHEMISTRY · FEBRUARY 2010

Impact Factor: 3.45 · DOI: 10.1016/j.ejmech.2010.02.027 · Source: PubMed

A computational study of the binding of 3-(arylidene) anabaseines to two major brain nicotinic acetylcholine receptors and to the acetylcholine binding protein

Svetoslav H. Slavov [a], Maksim Radzvilovits [a], Susan LeFrancois [b], Iva B. Stoyanova-Slavova [a], Ferenc Soti [b], William R. Kem [b,**], Alan R. Katritzky [a,*]

[a] Center for Heterocyclic Compounds, Department of Chemistry, University of Florida, Gainesville, FL 32611, USA
[b] Department of Pharmacology and Therapeutics, College of Medicine, University of Florida, Gainesville, FL 32610, USA

A B S T R A C T

Nicotinic acetylcholine receptors (nAChRs) have become targets for drug development in recent years. 3-(2,4-dimethoxybenzylidene)-anabaseine (DMXBA), which selectively stimulates the α7 nAChR, has been shown to alleviate some cognitive deficits associated with schizophrenia. In this paper we report an analysis of the interactions between 47 arylidene-anabaseines (including 45 benzylidene-anabaseines) and rat brain α7 and α4β2 nicotinic acetylcholine receptors, using three different modeling techniques, namely 2D-QSAR, 3D-QSAR and molecular docking to the *Aplysia californica* acetylcholine binding protein (AChBP), a water soluble, homomeric nAChR surrogate receptor with a known crystal structure. Our investigation indicates the importance of: (1) the nitrogen atom of the tetrahydropyridyl (THP) ring for hydrogen bond formation; (2) π–π interactions between the aromatic rings of the ligands and the nAChBP binding site; (3) molecular surface recognition expressed in terms of steric complimentarity. On the basis of the 3D-QSAR results, bulky substituents at positions 2 (and due to the rotational freedom also at position 6) and 4 of the benzylidene moiety, with highly electronegative atoms projecting approximately 3–3.5 Å away from the benzylidene ring at position 4 seem optimal for enhancing binding affinity to the α7 nAChR.

Keywords:
Nicotinic acetylcholine receptor
QSAR
AChBP
Docking
Anabaseine
DMBXA
GTS-21
Benzylidene-anabaseine

1. Introduction

Rational drug design requires knowledge of both the structure of the receptor and the ligand as isolated species, and also that of the ligand–receptor complex. With the increasing availability of crystal structures for many drug receptors, scientists working in the field of computer aided drug design have changed their focus from developing simple descriptor–property relationships to the detailed investigation of the more complex ligand–receptor interactions. The docking procedure responsible for fitting ligand and receptor together in 3D-space is attracting much attention, and there is a growing number of software packages available to enable this important process in drug design [1].

Although investigation of how drugs work on central nervous system (CNS) receptors has advanced rapidly in recent years, it is still hampered by the fact that most of these receptors are large membrane proteins that are difficult to crystallize for X-ray diffraction studies or have broadened NMR spectral resonance peaks. Nicotinic acetylcholine receptors (nAChRs) are such membrane proteins. The nAChRs belong to a superfamily of pentameric ligand-gated ion channel (LGIC) receptors that also includes GABA-A, 5HT3 and glycine-activated ionotropic ion channels. The various nAChRs are composed of a number of different combinations of subunits. For example, the most abundant subtypes in the brain are the homomeric α7 subtype (α-bungarotoxin sensitive) and the heteromeric α4β2 subtype. To date seventeen different nAChR subunits have been identified: five (α1, β1, γ, δ, ε) expressed in skeletal muscle cells and twelve (α2-10, β2-4) predominantly in nerve cells. Vertebrate nAChRs are always cation channels permeable to Na^+ and K^+ and, to varying extents, Ca^{2+} ions [2]. A low resolution electron microscopic (4 Å) structure of a heteromeric muscle nAChR is the best nAChR structure available at this time [3].

Nicotine binds exclusively to these LGIC receptors, which are normally activated by the ubiquitous neurotransmitter acetylcholine (ACh), making them important targets for the development of new types of drugs. Understanding the molecular interactions of nicotinic ligands with some nAChRs may, by facilitating the design of new drugs for treating nicotine dependence, reduce the prevalence of smoking-related diseases, which are responsible for

* Corresponding author. Tel.: +1 352 392 0554; fax: +1 352 392 9199.
** Corresponding author. Tel.: +1 352 392 0669; fax: +1 352 392 9696.
E-mail addresses: wrkem@ufl.edu (W.R. Kem), katritzky@chem.ufl.edu (A.R. Katritzky).

approximately 20% of deaths each year in developed countries [4]. Also, accumulating evidence for abnormal CNS nAChR expression in neurodevelopmental (schizophrenia) and neurodegenerative diseases (Alzheimer's and Parkinson's diseases) has stimulated pharmaceutical interest in development of nAChR subtype selective agonists to enhance mental functions, particularly sensory gating, attention and cognition [5,6]. Recent studies have demonstrated that some arylidene derivatives of a marine toxin, anabaseine, can selectively stimulate the α7 nAChR [7–9]. This receptor has exceptionally high Ca permeability; actually, it can be considered to be a calcium channel unique in its ability to pass Ca ions even at normal resting membrane potentials, when other Ca channels are inactive. The ability of this nAChR to cause localized and limited elevation of intracellular Ca levels probably explains its ability to mediate the neuroprotective [10] and cognition enhancing effects [11–13].

In spite of an ability to express and study mammalian nAChRs in cultured cells, application of rational drug design to these targets has been impeded by the unavailability of high resolution 3D structures of the receptors. However, the crystal structure of a soluble pentameric nAChR homolog, the acetylcholine binding protein (AChBP), was reported eight years ago [14]. Subsequently published crystal structures of this surrogate nAChR and its *Aplysia* homolog, occupied by agonists or antagonists have, coupled with mutagenesis studies on actual nAChRs, supplied a rather precise picture of how nicotinic ligands bind to the ACh recognition sites of nAChRs [15,16]. Quite recently, crystalline complexes of *Aplysia* AChBP with the marine toxin anabaseine [8] and two of its benzylidene-adducts, the drug candidate DMXBA and its active metabolite 4-OH-DMXBA [9], have also been solved at high resolution, affording much insight into the probable interactions of these ligands with α7 nAChRs [17].

How various substituents on the arylidene ring affect the interaction of anabaseine derivatives with the α7 nAChR is the major focus of this study. We have used a variety of computational methods to determine the 2D- and 3D-QSAR relationships for 47 arylidene-anabaseine (BA) compounds. For comparison, a 2D-QSAR relationship for K_is of $\alpha4\beta2$ neuronal receptors which are inhibited to varying degrees by this type of compounds was also derived. A number of the BAs were docked with the nAChR receptor surrogate *Aplysia* AChBP. The results of our study will hopefully lead to the design of new arylidene-anabaseine and other compounds that optimally activate this important brain nAChR.

2. Materials and methods

2.1. Synthesis and chemical characterization of Arylidene-Anabaseines

BAs were generally synthesized by the Kem-Soti laboratory as previously described [9,18]. In all the reactions the highest purity chemicals available (generally obtained from Sigma–Aldrich or Fisher) were used. To a mixture of anabaseine dihydrochloride monohydrate (101 mg, 0.4 mmole) and the appropriate benzaldehyde derivative (0.5 mmole) in dry ethanol (3 ml) one drop of concentrated hydrochloric acid was added and stirred under a very weak stream of dry argon gas in an oil bath of 70–75 °C overnight, if not given a stated time below. The system was protected from moisture with a Drierite tube. The mixture was then cooled overnight in a refrigerator. BA product purification proceeded according to one of these methods, as noted:

under argon atmosphere (to protect from moisture) and dried in a vacuum desiccator at room temperature overnight.

Method B. If the product did not crystallize, the solution was evaporated, dissolved in a small amount of water, basified with solid sodium hydrogen carbonate, extracted with dichloromethane, and evaporated. The crude product was subsequently purified by crystallization or silica gel chromatography. In some cases semipreparative SG HPLC using a hexane–alcohol (variable)–0.5% diethylamine solvent system with a linearly increasing concentration of either isopropanol or ethanol was used for final compound purification.

2.1.1. 3-(4-Aminobenzylidene)anabaseine (1.1)

Method B. ^{1}H NMR (DMSO-d_6, TMS, 300 MHz, δ ppm): 8.61–8.57 (2H, m), 7.79 (1H, dt, J = 8.1, 2.1 Hz), 7.42 (1H, ddd, J = 7.8, 5.1, 0.6 Hz), 7.08 (2H, d, J = 8.4 Hz), 6.55 (2H, d, J = 8.4 Hz), 6.36 (1H, s), 3.69 (2H, app t, J = 5.4 Hz), 3.32 (2H, s) 2.77 (2H, app td, J = 6.3, 1.5 Hz), 1.71 (2H, app quintet, J = 6.0 Hz). HRMS [ESI(+)-TOF-MS] calcd for $C_{17}H_{18}N_3$ $(M+H)^+$, Mr = 264.1495; found 264.1506.

2.1.2. 3-(4-t-Butoxybenzylidene)anabaseine (1.2)

Prepared by reaction of N,N-dimethylformamide di-tert-butyl acetal with compound **1.5** and purification by column chromatography, yield 20%. ^{1}H NMR ($CDCl_3$, TMS, 300 MHz, δ ppm): 8.74 (1H, dd, J = 2.4, 0.6 Hz), 8.63 (1H, dd, J = 4.8, 1.8 Hz), 7.81 (1H, dt, J = 8.1, 1.8 Hz), 7.32 (1H, ddd, J = 7.5, 4.8, 0.6 Hz), 7.23 (2H, d, J = 8.4 Hz), 6.98 (2H, d, J = 8.4 Hz), 6.60 (1H, s), 3.87 (2H, app t, J = 5.4 Hz), 2.85 (2H, app td, J = 6.6, 2.1 Hz), 1.84 (app quintet, J = 6.0 Hz), 1.37 (9H, s). HRMS [ESI(+)-TOF-MS] calcd for $C_{21}H_{25}N_2O$ $(M+H)^+$, Mr = 321.1961; found 321.1952.

2.1.3. 3-(4-Trifluoromethoxybenzylidene)anabaseine bishydrochloride (1.3)

Method A, yield 25%. ^{1}H NMR (DMSO-d_6, TMS, 300 MHz, δ ppm): 8.96–8.90 (2H, m), 8.20 (1H, dt, J = 8.1, 1.8 Hz), 7.79–7.70 (3H, m), 7.51 (2H, d, J = 8.1 Hz), 7.30 (1H, s), 3.85 (2H, app t, J = 5.7 Hz), 2.97 (2H, app t, J = 6.0 Hz), 2.04 (2H, app quintet, J = 6.0). Anal. Calcd for $C_{18}H_{17}F_3Cl_2N_2O$: C, 53.35; H, 4.23; N, 6.91. Found: C, 53.45; H, 4.33; N, 6.85.

2.1.4. 3-(4-Methylaminobenzylidene)anabaseine bishydrochloride (1.4)

Method A, yield 68%. ^{1}H NMR (DMSO-d_6, TMS, 300 MHz, δ ppm): 8.96 (1H, dd, J = 4.8, 1.5 Hz), 8.90 (1H, d, J = 1.8 Hz), 8.23 (1H, dt, J = 8.1, 1.8 Hz), 7.83 (1H, dd, J = 8.1, 5.4 Hz), 7.50 (2H, d, J = 9.0 Hz), 7.03 (1H, s), 6.66 (2H, d, J = 9.0 Hz), 3.76–3.36 (2H, m), 2.96 (2H, app t, J = 6.0 Hz), 2.05 (2H, app quintet, J = 5.7 Hz). HRMS [ESI(+)-TOF-MS] calcd for $C_{18}H_{20}N_3$ $(M+H)^+$, Mr = 278.1652; found 278.1640.

2.1.5. 3-(4-Hydroxybenzylidene)anabaseine bishydrochloride (1.5)

Reaction time 9 days, Method A, yield 95%. ^{1}H NMR (DMSO-d_6, TMS, 300 MHz, δ ppm): 8.91 (1H, dd, J = 5.1, 1.5 Hz), 8.85 (1H, dd, J = 2.1, 0.9 Hz), 8.14 (1H, dt, J = 7.8, 1.8 Hz), 7.73 (1H, ddd, J = 8.1, 4.8, 0.9 Hz), 7.54 (2H, d, J = 8.7 Hz), 7.13 (1H, s), 6.92 (2H, d, J = 8.7 Hz), 3.78 (2H, app t, J = 5.4 Hz), 2.94 (2H, app t, J = 6.0 Hz), 2.05 (2H, app quintet, J = 5.7 Hz). Anal. Calcd for $C_{17}H_{18}Cl_2N_2O$: C, 60.54; H, 5.38; N, 8.31. Found: C, 60.32; H, 5.25; N, 8.21.

2.1.6. 3-(4-Methoxybenzylidene)anabaseine bishydrochloride (1.6)

Method A, yield 93%. ^{1}H NMR (DMSO-d_6, TMS, 300 MHz, δ ppm): 8.94 (1H, dd, J = 5.1, 1.8 Hz), 8.91 (1H, d, J = 2.1 Hz), 8.21 (1H, dt, J = 8.1, 1.8 Hz), 7.78 (1H, dd, J = 8.1, 5.1 Hz), 7.64 (2H, d,

app t, J = 5.7 Hz), 3.00 (2H, app t, J = 6.0 Hz), 2.05 (2H, app quintet, J = 6.6 Hz). Anal. Calcd for $C_{18}H_{20}Cl_2N_2O$: C, 61.55; H, 5.74; N, 7.97. Found: C, 61.54; H, 5.60; N, 7.96.

*2.1.7. 3-(4-Methylbenzylidene)anabaseine bishydrochloride (**1.7**)*

Method A, yield 67%. ^{1}H NMR (DMSO-d_6, TMS, 300 MHz, δ ppm): 8.93 (1H, dd, J = 5.1, 1.8 Hz), 8.89 (1H d, J = 2.1 Hz), 8.19 (1H, dt, J = 7.8, 2.1 Hz), 7.75 (1H, dd, J = 7.8, 5.1 Hz), 7.52 (2H, d, J = 8.4 Hz), 7.33 (2H, d, J = 8.1 Hz), 7.21 (1H, s), 3.82 (2H, app t, J = 5.4 Hz), 3.00 (2H, app t, J = 5.7 Hz), 2.37 (3H, s), 2.04 (2H, app quintet, J = 6.0 Hz). HRMS [ESI(+)-TOF-MS] calcd for $C_{18}H_{19}N_2$ $(M+H)^+$, Mr = 263.1543; found 263.1568.

*2.1.8. 3-(4-Methylthiobenzylidene)anabaseine bishydrochloride (**1.8**)*

Method A, yield 95%. ^{1}H NMR (DMSO-d_6, TMS, 300 MHz, δ ppm): 9.01–8.93 (2H, m), 8.29 (1H, dt, J = 7.8, 1.8 Hz), 7.84 (1H, dd, J = 7.8, 5.1 Hz), 7.57 (2H, d, J = 8.7 Hz), 7.37 (2H, d, J = 8.7 Hz), 7.21 (1H, s), 3.82 (2H, app t, J = 5.7 Hz), 3.00 (2H, app t, J = 5.7 Hz), 2.53 (3H, s), 2.05 (2H, app quintet, J = 5.7 Hz). Anal. Calcd for $C_{18}H_{20}Cl_2N_2S$: C, 58.85; H, 5.49; N, 7.63. Found: C, 58.80; H, 5.37; N, 7.56.

*2.1.9. 3-(4-Cyanobenzylidene)anabaseine (**1.9**)*

Reaction time 2 days, Method B, purified by recrystallization from benzene, yield 20%, mp.: 160.5–161.5 °C. ^{1}H NMR ($CDCl_3$, TMS, 300 MHz, δ ppm): 8.75 (1H, dd, J = 2.1, 0.6 Hz), 8.65 (1H, dd, J = 4.8, 1.5 Hz), 7.83 (1H, dt, J = 8.1, 1.8 Hz), 7.65 (2H, d, J = 8.4 Hz), 7.39 (2H, d, J = 8.4 Hz), 7.35 (1H, ddd, J = 7.8, 5.1, 0.9 Hz), 6.65 (1H, s), 3.93 (2H, app t, J = 5.4 Hz), 2.81 (2H, app td, J = 6.6, 2.1 Hz), 1.85 (app quintet, J = 6.3 Hz). Anal. Calcd for $C_{18}H_{15}N_3$: C, 79.10; H, 5.53; N, 15.37. Found: C, 79.05; H, 5.46; N, 15.41.

*2.1.10. 3-(4-n-Propylbenzylidene)anabaseine bishydrochloride (**1.10**)*

Using 4-n-propylbenzaldehyde diethyl acetal, Method A, yield 57%. ^{1}H NMR (DMSO-d_6, TMS, 300 MHz, δ ppm): 8.98–8.92 (2H, m), 8.25 (1H, dt, J = 8.4, 1.8 Hz), 7.80 (1H, ddd, J = 7.8, 5.1, 0.6 Hz), 7.54 (2H, d, J = 8.1 Hz), 7.34 (2H, d, J = 8.4 Hz), 7.22 (1H, s), 3.82 (2H, app t, J = 5.7 Hz), 3.00 (2H, app t, J = 6.0 Hz), 2.62 (2H, t, J = 7.8 Hz), 2.05 (2H, app quintet, J = 6.0 Hz), 1.60 (2H, sextet, J = 7.5 Hz), 0.89 (3H, t, J = 7.2 Hz). Anal. Calcd for $C_{20}H_{24}Cl_2N_2$: C, 66.12; H, 6.66; N, 7.71. Found: C, 66.07; H, 6.74; N, 7.75.

*2.1.11. 3-(4-Acetoxybenzylidene)anabaseine (**1.11**)*

Prepared by acetylation of compound **1.5** with acetic anhydride and purified by column chromatography, yield 72%. ^{1}H NMR ($CDCl_3$, TMS, 300 MHz, δ ppm): 8.74 (1H, d, J = 1.5 Hz), 8.64 (1H, dd, J = 4.8, 1.5 Hz), 7.82 (1H, dt, J = 7.8, 1.8 Hz), 7.38–7.28 (3H, m), 7.09 (2H, d, J = 8.7 Hz), 6.63 (1H, s), 3.89 (2H, app t, J = 5.7 Hz), 2.83 (2H, app td, J = 5.1, 1.8 Hz), 2.31 (3H, s), 1.84 (app quintet, J = 6.0 Hz). Anal. Calcd for $C_{19}H_{18}N_2O_2$: C, 74.49; H, 5.92; N, 9.14. Found: C, 74.20; H, 6.09; N, 9.22.

*2.1.12. 3-(4-Morpholinobenzylidene)anabaseine bishydrochloride (**1.12**)*

Method A, yield 73%, mp.: 247–250 °C. ^{1}H NMR (DMSO-d_6, TMS, 300 MHz, δ ppm): 8.96 (1H, dd, J = 5.1, 1.5 Hz), 8.91 (1H, d, J = 2.4 Hz), 8.24 (1H, dt, J = 8.1, 1.8 Hz), 7.82 (1H, dd, J = 8.1, 5.4 Hz), 7.57 (2H, d, J = 9.0 Hz), 7.11 (1H, s), 7.03 (2H, d, J = 9.3 Hz), 3.80–3.67 (6H, m), 3.40–3.31 (4H, m), 2.99 (2H, app t, J = 5.7 Hz), 2.05 (2H, app quintet, J = 5.7 Hz). HRMS [ESI(+)-TOF-MS] calcd for $C_{21}H_{24}N_3O$ $(M+H)^+$, Mr = 334.1914; found 334.1912.

2.1.13. 3-(4-Dimethylaminobenzylidene)anabaseine

*2.1.14. 3-(4-Difluoromethoxybenzylidene)anabaseine bishydrochloride (**1.14**)*

Method A, yield 67%, mp.: 205–210 °C (decomp.). ^{1}H NMR (DMSO-d_6, TMS, 300 MHz, δ ppm): 8.99–8.92 (2H, m), 8.25 (1H, dt, J = 8.1, 1.8 Hz), 7.80 (1H, dd, J = 7.8, 5.1 Hz), 7.70 (2H, d, J = 8.7, Hz), 7.26 (1H, t, J = 73.2 Hz, $OCHF_2$), 7.31 (2H, d, J = 8.7 Hz), 7.17 (1H, s), 3.83 (2H, app t, J = 5.7 Hz), 2.98 (2H, app t, J = 5.7 Hz), 2.05 (2H, app quintet, J = 6.0 Hz). Anal. Calcd for $C_{18}H_{18}F_2Cl_2N_2O$: C, 55.83; H, 4.69; N, 7.23. Found: C, 55.79; H, 4.78; N, 7.17.

*2.1.15. 3-(4-Chlorobenzylidene)anabaseine bishydrochloride (**1.15**)*

Method A, yield 69%, ^{1}H NMR (DMSO-d_6, TMS, 300 MHz, δ ppm): 8.97–8.91 (2H, m), 8.24 (1H, dt, J = 8.1, 1.8 Hz), 7.78 (1H, dd, J = 7.8, 5.1 Hz), 7.61 (4H, AB q), 7.26 (1H, s), 3.84 (2H, app t, J = 5.7 Hz), 2.96 (2H, app t, J = 5.7 Hz), 2.04 (app quintet, J = 6.0 Hz). Anal. Calcd for $C_{17}H_{17}Cl_3N_2$: C, 57.40; H, 4.82; N, 7.88. Found: C, 57.21; H, 4.90; N, 7.81.

*2.1.16. 3-[4-(1H-1,2,4-Triazol-1-yl)-benzylidene]anabaseine trishydrochloride (**1.16**)*

Method A, yield 71%, mp.: 195–200 °C. ^{1}H NMR (DMSO-d_6, TMS, 300 MHz, δ ppm): 9.47 (1H, s), 8.98–8.93 (2H, m), 8.32 (1H, s), 8.25 (1H, dt, J = 8.1, 1.8 Hz), 8.04 (2H, d, J = 8.7 Hz), 7.86–7.75 (3H, m), 7.31 (1H, s), 3.85 (2H, app t, J = 5.7 Hz), 3.03 (2H, app t, J = 5.7 Hz), 2.07 (2H, app quintet, J = 6.0 Hz), contains ~3.8% of ethanol. HRMS [ESI(+)-TOF-MS] calcd for $C_{19}H_{18}N_5$ $(M+H)^+$, Mr = 316.1557; found 316.1583.

*2.1.17. 3-(4-Acetamidobenzylidene)anabaseine bishydrochloride (**1.17**)*

Method A, but concentrated hydrochloric acid was not added, yield 87%. ^{1}H NMR (DMSO-d_6, TMS, 300 MHz, δ ppm): 10.58 (1H, s), 8.97 (1H, dd, J = 5.4, 1.5 Hz), 8.94 (1H, d, J = 1.8 Hz), 8.26 (1H, dt, J = 7.8, 1.8 Hz), 7.82 (1H, dd, J = 7.8, 4.8 Hz), 7.77 (2H, d, J = 8.7 Hz), 7.61 (2H, d, J = 8.7 Hz), 7.16 (1H, s), 3.81 (2H, app t, J = 5.4 Hz), 3.01 (2H, app t, J = 5.7 Hz), 2.09 (3H, s), 2.06 (2H, app quintet, J = 5.4 Hz). Anal. Calcd for $C_{19}H_{21}Cl_2N_3O$: C, 60.32; H, 5.60; N, 11.11. Found: C, 59.97; H, 5.76; N, 11.00.

*2.1.18. 3-[4-bis(2-Hydroxyethyl)aminobenzylidene]anabaseine bishydrochloride (**1.18**)*

Method A, yield, 59%. ^{1}H NMR (DMSO-d_6, TMS, 300 MHz, δ ppm): 8.93 (1H, dd, J = 5.1, 1.8 Hz), 8.86 (1H, d, J = 1.8 Hz), 8.17 (1H, dt, J = 8.1, 1.8 Hz), 7.78 (1H, dd, J = 7.8, 5.1 Hz), 7.51 (2H, d, J = 9.0 Hz), 7.05 (1H, s), 6.84 (2H, d, J = 9.0 Hz), 3.72 (2H, br s), 3.56 (8H, s), 2.97 (2H, app t, J = 6.0 Hz), 2.05 (2H, app quintet, J = 5.4 Hz). HRMS [ESI(+)-TOF-MS] calcd for $C_{21}H_{26}N_3O_2$ $(M+H)^+$, Mr = 352.2020; found 352.2017.

*2.1.19. 3-(4-Pivaloyloxybenzylidene)anabaseine (**1.19**)*

Prepared by acylation of compound **1.5** with pivalic anhydride and purified by column chromatography, yield 89%. ^{1}H NMR ($CDCl_3$, TMS, 300 MHz, δ ppm): 8.75 (1H, d, J = 1.8 Hz), 8.65 (1H, dd, J = 4.8, 1.8 Hz), 7.83 (1H, dt, J = 7.8, 1.8 Hz), 7.35 (1H, ddd, J = 7.8, 5.1, 0.9 Hz), 7.31 (2H, d, J = 8.7 Hz), 7.06 (2H, d, J = 8.7 Hz), 6.64 (1H, s), 3.89 (2H, app t, J = 6.3 Hz), 2.82 (2H, app td, J = 6.3, 1.8 Hz), 1.84 (2H, app quintet, J = 6.3 Hz), 1.36 (9H, s), contains ~2% of ethanol. HRMS [ESI(+)-TOF-MS] calcd for $C_{22}H_{25}N_2O_2$ $(M+H)^+$, Mr = 349.1911; found 349.1900.

*2.1.20. 3-(4-Acetylbenzylidene)anabaseine bishydrochloride (**1.20**)*

Method A, yield 97%, ^{1}H NMR (DMSO-d_6, TMS, 300 MHz, δ ppm): 8.98–8.92 (2H, m), 8.26 (1H, dt, J = 8.1, 2.1 Hz), 8.05 (2H, d, J = 8.4 Hz), 7.79 (1H, dd, J = 8.1, 5.1 Hz), 7.72 (2H, d, J = 8.4 Hz), 7.32

(app quintet, J = 5.7 Hz). Anal. Calcd for $C_{19}H_{20}Cl_2N_2O$: C, 62.82; H, 5.55; N, 7.71. Found: C, 62.51; H, 5.72; N, 7.60.

2.1.21. 3-(4-n-Butoxybenzylidene)anabaseine bishydrochloride (1.21)

Method A, yield 64%, ^{1}H NMR (DMSO-d_6, TMS, 300 MHz, δ ppm): 8.94 (1H, dd, J = 5.1, 1.5 Hz), 8.89 (1H, d, J = 2.1 Hz), 8.19 (1H, dt, J = 8.1, 1.8 Hz), 7.77 (1H, dd, J = 8.1, 4.8 Hz), 7.62 (2H, d, J = 9.0 Hz), 7.19 (1H, s), 7.07 (2H, d, J = 8.7 Hz), 4.06 (2H, t, J = 6.6 Hz), 3.80 (2H, app t, J = 5.7 Hz), 2.99 (2H, app t, J = 5.7 Hz), 2.05 (2H, app quintet, J = 6.0 Hz), 1.71 (2H, quintet, J = 6.9 Hz), 1.43 (2H, sextet, J = 7.5 Hz), 0.93 (3H, t, J = 7.5 Hz). Anal. Calcd for $C_{21}H_{26}Cl_2N_2O$: C, 64.12; H, 6.66; N, 7.12. Found: C, 63.99; H, 6.95; N, 7.09.

2.1.22. 3-(2-Acetoxybenzylidene)anabaseine (1.22)

Prepared by acetylation of 3-(2-hydroxybenzylidene)anabaseine with acetic anhydride and purified by column chromatography, yield 78%, ^{1}H NMR ($CDCl_3$, TMS, 300 MHz, δ ppm): 8.66 (1H, d, J = 1.8 Hz), 8.57 (1H, dd, J = 4.8, 1.5 Hz), 7.73 (1H, dt, J = 8.1, 1.8 Hz), 7.36–7.15 (4H, m), 7.01 (1H, dd, J = 7.8, 1.5 Hz), 6.48 (1H, s), 3.85 (2H, app t, J = 5.7 Hz), 2.63 (2H, app td, J = 6.6, 1.8 Hz), 2.11 (3H, s), 1.76 (2H, app quintet, J = 6.3 Hz). HRMS [ESI(+)-TOF-MS] calcd for $C_{17}H_{17}N_2O$ $(M+H)^+$, Mr = 265.1335; found 265.1315.

2.1.23. 3-(2-Trifluoromethoxybenzylidene)anabaseine bishydrochloride (1.23)

Reaction time 10 days, Method A, yield 60%. ^{1}H NMR (DMSO-d_6, TMS, 300 MHz, δ ppm): 8.96–8.90 (2H, m), 8.21 (1H, dt, J = 8.4, 1.8 Hz), 7.79–7.72 (2H, m), 7.70–7.48 (3H, m), 7.18 (1H, s), 3.88 (2H, app t, J = 5.7 Hz), 2.87 (2H, app t, J = 5.7 Hz), 2.04 (2H, app quintet, J = 5.7 Hz). Anal. Calcd for $C_{18}H_{17}F_3Cl_2N_2O$: C, 53.35; H, 4.23; N, 6.91. Found: C, 53.10; H, 4.55; N, 6.84

2.1.24. 3-(2-Difluoromethoxybenzylidene)anabaseine bishydrochloride (1.24)

Method A, yield 77%. ^{1}H NMR (DMSO-d_6, TMS, 300 MHz, δ ppm): 8.96–8.90 (2H, m), 8.21 (1H, dt, J = 8.1, 1.8 Hz), 7.75 (1H, ddd, J = 7.8, 5.1, 0.6 Hz), 7.68 (1H, dd, J = 7.5, 1.8 Hz), 7.60 (1H, td, J = 7.8, 1.8 Hz), 7.41 (1H, app t, J = 7.5 Hz), 7.31 (1H, d, J = 7.8 Hz), 7.24 (1H, s), 7.20 (1H, t, J = 73.5 Hz, $OCHF_2$), 3.87 (2H, app t, J = 5.4 Hz), 2.90 (2H, app t, J = 5.7 Hz), 2.04 (2H, app quintet, J = 6.0 Hz). Anal. Calcd for $C_{18}H_{18}F_2Cl_2N_2O$: C, 55.83; H, 4.69; N, 7.23. Found: C, 55.82; H, 4.82; N, 7.21.

2.1.25. 3-(2-Pivaloyloxybenzylidene)anabaseine (1.25)

Prepared by acylation of 3-(2-hydroxybenzylideen)anabaseine with pivalic anhydride and purified by column chromatography, yield 91%, ^{1}H NMR ($CDCl_3$, TMS, 300 MHz, δ ppm): 8.71 (1H, d, J = 1.5 Hz), 8.62 (1H, dd, J = 4.8, 1.5 Hz), 7.77 (1H, dt, J = 8.1, 1.8 Hz), 7.39 (1H, dd, J = 7.8, 1.8 Hz), 7.35–7.23 (3H, m), 7.02 (1H, dd, J = 7.8, 1.5 Hz), 6.58 (1H, s), 3.90 (2H, app t, J = 5.7 Hz), 2.76–2.67 (2H, m), 1.81 (2H, app quintet, J = 6.3 Hz). HRMS [ESI(+)-TOF-MS] calcd for $C_{22}H_{25}N_2O_2$ $(M+H)^+$, Mr = 349.1911; found 349.1903.

2.1.26. 3-(3-Methoxybenzylidene)anabaseine bishydrochloride (1.26)

Method A, yield 80%. ^{1}H NMR (DMSO-d_6, TMS, 300 MHz, δ ppm): 8.97–8.91 (2H, m), 8.24 (1H, dt, J = 8.1, 1.8 Hz), 7.79 (1H, dd, J = 7.8, 5.1 Hz), 7.44 (1H, t, J = 7.8 Hz), 7.25 (1H, s), 7.19 (1H, d, J = 7.8 Hz) 7.15–7.06 (2H, m), 3.84 (2H, app t, J = 5.4 Hz), 3.77 (3H, s), 3.00 (2H, app t, 5.7 Hz), 2.04 (2H, app quintet, J = 6.00 Hz). Anal.

2.1.27. 3-(3-Hydroxybenzylidene)anabaseine bishydrochloride (1.27)

Method A, yield 92%. ^{1}H NMR (DMSO-d_6, TMS, 300 MHz, δ ppm): 8.94 (1H, dd, J = 4.8, 1.2 Hz), 8.92 (1H, d, J = 2.1 Hz), 8.22 (1H, dt, J = 8.1, 1.8 Hz), 7.78 (1H, dd, J = 7.8, 5.1 Hz), 7.30 (1H, t, J = 7.8 Hz), 7.16 (1H, s), 7.04–6.90 (3H, m), 3.83 (2H, app t, J = 5.7 Hz), 2.98 (2H, app t, J = 5.7 Hz), 2.04 (2H, app quintet, J = 6.0 Hz). Anal. Calcd for $C_{18}H_{20}Cl_2N_2O \times H_2O$: C, 57.47; H, 5.67; N, 7.89. Found: C, 57.41; H, 5.80; N, 7.80.

2.1.28. 3-(2,4-Dimethoxybenzyl)anabasine (1.28)

Prepared by hydrogenation (at room temperature and room pressure) over 10% Pd/C from compound **1.42** in ethanolic solution followed by purification of the free base by column chromatography and recrystallization from n-hexane, yield 14%, mp: 95–96.5 °C. ^{1}H NMR ($CDCl_3$, TMS, 300 MHz, δ ppm): 8.62 (1H, d, J = 2.1 Hz), 8.49 (1H, dd, J = 5.1, 1.8 Hz), 7.70 (1H, dm, J = 7.8 Hz), 7.27 (1H, ddd, J = 7.8, 4.8, 0.6 Hz), 6.83–6.77 (1H, m), 6.35–6.30 (2H, m), 4.05 (1H, d, J = 2.7 Hz), 3.74 (3H, s), 3.61 (3H, s), 3.30 (1H, dm, J = 11.4 Hz), 2.83 (1H, td, J = 11.7, 2.7 Hz), 2.67 (1H, td, J = 12.6, 2.1 Hz), 2.22–2.09 (2H, m), 1.99–1.76 (2H, m), 1.75–1.63 (1H, m), 1.60–1.38 (2H, m). Anal. Calcd for $C_{19}H_{24}N_2O_2$: C, 73.05; H, 7.74; N, 8.97. Found: C, 72.93; H, 8.22; N, 8.95.

2.1.29. 3-(2-Methoxy-4-glucuronidobenzylidene)anabaseine (1.29)

Prepared from compound **1.43** by reaction with acetobromo-α-D-glucuronic acid methyl ester in methanolic lithium hydroxide solution, removal of the protecting groups and purification of the raw product by HPLC. ^{1}H NMR (DMSO-d_6, TMS, 300 MHz, δ ppm): 8.90 (1H, dd, J = 5.1, 1.8 Hz), 8.83 (1H, d, J = 1.8 Hz), 8.08 (1H, dt, J = 8.4, 2.1 Hz), 7.69 (1H, dd, J = 7.8, 5.4 Hz), 7.60 (1H, d, J = 9.0 Hz), 7.32 (1H, s), 6.79 (1H, dd, J = 8.7, 2.4 Hz), 6.71 (1H, d, J = 2.4 Hz), 5.24 (1H, d, J = 7.2 Hz), 3.98 (1H, d, J = 9.3 Hz), 3.70 (s), some multiplets at the water peak, 2.93 (2H, app t), 2.03 (2H, app quintet). HRMS [ESI(-)-TOF-MS] calcd for $C_{24}H_{25}N_2O_8$ $(M-H)^-$, Mr = 469.1616; found 469.1627.

2.1.30. 3-(2-i-Propoxy-4-methoxybenzylidene)anabaseine (1.30)

Method B, yield 99%. ^{1}H NMR ($CDCl_3$, TMS, 300 MHz, δ ppm): 8.76 (1H, s), 8.62 (1H dm, J = 4.8 Hz), 7.83 (1H, dm, J = 8.1 Hz), 7.34–7.22 (2H, m), 6.82 (1H, s), 6.49 (1H, dm, J = 8.7 Hz), 6.43 (1H, s), 4.41 (1H, heptet, J = 6.3 Hz), 3.90 (2H, app t, J = 5.1 Hz), 3.80 (3H, s), 2.76 (2H, app tm, J = 6.3 Hz), 1.84 (1H, app quintet, J = 6.3 Hz), 1.22 (6H, d, J = 6.3 Hz). HRMS [ESI(+)-TOF-MS] calcd for $C_{21}H_{25}N_2O_2$ $(M+H)^+$, Mr = 337.1911; found 337.1898.

2.1.31. 3-[2-(Pentan-3-yloxy)-4-methoxybenzylidene]anabaseine (1.31)

Method B, yield 99%. ^{1}H NMR ($CDCl_3$, TMS, 300 MHz, δ ppm): 8.73 (1H, s), 8.59 (1H, dm, J = 5.1 Hz), 7.80 (1H, dm, J = 7.6 Hz), 7.34–7.22 (2H, m), 6.86 (1H, s), 6.48 (1H, dm, J = 8.9 Hz), 6.40 (1H, s), 4.03 (1H, quintet, J = 6.3 Hz), 3.89 (2H, app t, J = 6.3 Hz), 3.80 (3H, s), 2.78 (2H, app tm, J = 6.3 Hz), 1.83 (2H, app quintet, J = 6.3 Hz), 1.56 (4H, quintet, J = 6.3 Hz), 0.79 (6H, t, J = 7.2 Hz). HRMS [ESI(+)-TOF-MS] calcd for $C_{23}H_{29}N_2O_2$ $(M+H)^+$, Mr = 365.2224; found 365.2218.

2.1.32. 3-(2-Acetoxy-4-methoxybenzylidene)anabaseine (1.32)

Prepared from compound **1.44** by acetylation with acetic anhydride and purification by column chromatography, yield 8%. ^{1}H NMR ($CDCl_3$, TMS, 300 MHz, δ ppm): 8.71 (1H, d, J = 2.1 Hz), 8.63 (1H, dd, J = 4.8, 1.5 Hz), 7.78 (1H, dt, J = 7.8, 2.1 Hz), 7.37–7.29 (2H, m), 6.81 (1H, dd, J = 8.7, 2.7 Hz), 6.63 (1H, d, J = 2.7 Hz), 6.48 (1H, s), 3.89 (2H, app t, J = 5.7 Hz), 3.81 (3H, s), 2.76–2.68 (2H, m),

MS] calcd for $C_{20}H_{21}N_2O_3$ $(M+H)^+$, Mr = 337.1547; found 337.1546.

*2.1.33. 3-(2-Hydroxy-4-diethylaminobenzylidene)anabaseine (**1.33**)*

Method B, yield 29%. ^{1}H NMR (DMSO-d_6, TMS, 300 MHz, δ ppm): 9.27 (1H br s), 8.59–8.55 (2H, m), 7.78 (1H, dt, J = 7.5, 2.1 Hz), 7.41 (1H, ddd, J = 7.5, 4.8, 0.6 Hz), 7.23 (1H, d, J = 8.7 Hz), 6.73 (1H, s), 6.19 (1H, dd, J = 8.7, 2.4 Hz), 6.12 (1H, d, J = 2.4 Hz), 3.70 (2H, app t, J = 5.4 Hz), 3.28 (4H, q, J = 6.9 Hz), 2.74 (2H, app t, J = 5.7 Hz), 1.71 (2H, app quintet, J = 6.3 Hz), 1.08 (6H, t, J = 6.9 Hz). HRMS [ESI(+)-TOF-MS] calcd for $C_{21}H_{26}N_3O$ $(M+H)^+$, Mr = 336.2070; found 336.2075.

*2.1.34. 3-(2,6-Dimethyl-4-hydroxybenzylidene)anabaseine (**1.34**)*

Method B, purified by column chromatography, yield 64%. ^{1}H NMR ($CDCl_3$, TMS, 300 MHz, δ ppm): 8.77 (1H, dd, J = 2.4, 0.6 Hz), 8.64 (1H, dd, J = 4.8, 1.5 Hz), 7.94 (1H, dt, J = 7.8, 1.8 Hz), 7.40 (1H, ddd, J = 7.8, 5.1, 0.9 Hz), 6.53 (1H, s), 6.50 (2H, s), 3.90 (2H, app t, J = 5.4 Hz), 2.27–2.18 (2H, m), 2.00 (6H, s), 1.77 (2H, app quintet, J = 6.6 Hz). Anal. Calcd for $C_{19}H_{20}N_2O$: C, 78.05; H, 6.90; N, 9.58. Found: C, 77.83; H, 7.29; N, 9.57.

*2.1.35. 3-(3,5-Dimethyl-4-hydroxybenzylidene)anabaseine bishydrochloride (**1.35**)*

Method A, yield 74%. ^{1}H NMR (DMSO-d_6, TMS, 300 MHz, δ ppm): 8.94 (1H, dd, J = 5.1, 1.8 Hz), 8.88 (1H, dd, J = 5.4, 0.6 Hz), 8.18 (1H, dt, J = 7.8, 1.8 Hz), 7.78 (1H, ddd, J = 7.8, 5.1 0.9 Hz), 7.30 (2H, s), 7.06 (1H, s), 3.78 (2H, app t, J = 5.4 Hz), 3.01 (2H, app t, J = 6.0 Hz), 2.19 (6H, s), 2.05 (2H, app quintet, J = 6.0 Hz). Anal. Calcd for $C_{19}H_{22}Cl_2N_2O$: C, 62.47; H, 6.07; N, 7.67. Found: C, 62.11; H, 6.00; N, 7.59.

*2.1.36. 3-(2,4,6-Trimethylbenzylidene)anabaseine bishydrochloride (**1.36**)*

Method A. ^{1}H NMR (DMSO-d_6, TMS, 300 MHz, δ ppm): 8.95–8.90 (2H, m), 8.23–8.17 (1H, m), 7.75 (1H, ddd, J = 8.1, 5.1, 0.9 Hz), 7.25 (1H, s), 6.94 (2H, s), 3.85 (2H, app t, J = 5.7 Hz), 2.38–2.30 (2H, m), 2.25 (3H, s), 2.10 (6H, s), 2.03–1.92 (2H, m). HRMS [ESI(+)-TOF-MS] calcd for $C_{20}H_{23}N_2$ $(M+H)^+$, Mr = 291.1856; found 291.1861.

*2.1.37. 3-(2,4,6-Trimethoxybenzylidene)anabaseine bishydrochloride (**1.37**)*

Method A. ^{1}H NMR (DMSO-d_6, TMS, 300 MHz, δ ppm): 8.92 (1H, dd, J = 4.8, 1.5 Hz), 8.85 (1H, d, J = 2.1 Hz), 8.12 (1H, dt, J = 8.1, 2.1 Hz), 7.74 (1H, dd, J = 7.8, 5.1 Hz), 7.05 (1H, s), 6.33 (2H, s), 3.85 (3H, s), 3.82 (2H, app t, J = 6.0 Hz), 3.79 (6H, s), ~2.5 (2H, under the DMSO signal), 1.97 (2H, app quintet, J = 6.0 Hz). Anal. Calcd for $C_{20}H_{24}Cl_2N_2O_3$: C, 58.40; H, 5.88; N, 6.81. Found: C, 58.08; H, 5.86; N, 6.68.

*2.1.38. 3-(3,4,5-Trimethoxybenzylidene)anabaseine bishydrochloride (**1.38**)*

Method A, yield 88%. ^{1}H NMR (DMSO-d_6, TMS, 300 MHz, δ ppm): 8.96 (1H, dd, J = 5.1, 1.5 Hz), 8.92 (1H, d, J = 1.5 Hz), 8.22 (1H, dt, J = 8.1, 1.8 Hz), 7.80 (1H, ddd, J = 7.8, 5.1, 0.6 Hz), 7.21 (1H, s), 6.93 (2H, s), 3.85–3.75 (8H, m), 3.73 (3H, s), 3.06 (2H, app t, J = 5.7 Hz), 2.05 (2H, app quintet, J = 5.7 Hz), contains ~14% of ethanol. HRMS [ESI(+)-TOF-MS] calcd for $C_{20}H_{23}N_2O_3$ $(M+H)^+$, Mr = 339.1703; found 339.1711.

*2.1.39. 3-(3,4-Ethylenedioxybenzylidene)anabaseine bishydrochloride (**1.39**)*

J = 1.5 Hz), 8.21 (1H, dt, J = 8.1, 1.8 Hz), 7.79 (1H, dd, J = 7.8, 5.1 Hz), 7.24–7.11 (3H, m), 6.99 (1H, d, J = 8.4 Hz), 4.37–4.24 (4H, m), 3.79 (2H, app t, J = 5.7 Hz), 2.98 (2H, app t, J = 5.7 Hz), 2.04 (2H, app quintet, J = 6.0 Hz). Anal. Calcd for $C_{19}H_{20}Cl_2N_2O_2$: C, 60.17; H, 5.32; N, 7.39. Found: C, 59.83; H, 5.39; N, 7.29.

*2.1.40. 3-(3,4-Methylenedioxybenzylidene)anabaseine bishydrochloride (**1.40**)*

Method A, yield 96%, mp.: 236–238 °C. ^{1}H NMR (DMSO-d_6, TMS, 300 MHz, δ ppm): 8.94 (1H, dd, J = 5.1, 1.5 Hz), 8.90 (1H, d, J = 1.5 Hz), 8.20 (1H, dt, J = 8.1, 1.8 Hz), 7.78 (1H, dd, J = 8.1, 5.1 Hz), 7.26 (1H, d, J = 1.5 Hz), 7.20 (1H, dd, J = 8.4, 1.2 Hz), 7.16 (1H, s), 7.08 (1H, d, J = 8.1 Hz), 6.15 (2H, s), 3.80 (2H, app t, J = 5.4 Hz), 2.99 (2H, app t, J = 5.7 Hz), 2.04 (app quintet, J = 5.7 Hz). Anal. Calcd for $C_{18}H_{18}Cl_2N_2O_2$: C, 59.19; H, 4.97; N, 7.68. Found: C, 58.79; H, 4.95; N, 7.85.

*2.1.41. 3-(Benzylidene)anabaseine bishydrochloride (**1.41**)*

Method A, yield 53%, ^{1}H NMR (DMSO-d_6, TMS, 300 MHz, δ ppm): 8.98–8.92 (2H, m), 8.25 (1H, dt, J = 8.4, 1.5 Hz), 7.79 (1H, ddd, J = 7.8, 5.1, 0.6 Hz), 7.64–7.56 (2H, m), 7.55–7.48 (3H, m), 7.27 (1H, s), 3.84 (2H, app t, J = 5.7 Hz), 3.00 (2H, app t, J = 5.7 Hz), 2.05 (2H, app quintet, J = 6.0 Hz). HRMS [ESI(+)-TOF-MS] calcd for $C_{17}H_{17}N_2$ $(M+H)^+$, Mr = 249.1386; found 249.1395.

*2.1.42. 3-(2,4-Dimethoxybenzylidene)anabaseine bishydrochloride (**1.42**)*

Known compound [9].

*2.1.43. 3-(2-Methoxy-4-hydroxybenzylidene)anabaseine (**1.43**)*

Known compound [9].

*2.1.44. 3-(2-Hydroxy-4-methoxybenzylidene)anabaseine (**1.44**)*

Known compound [9].

*2.1.45. 3-(2,4-Dihydroxybenzylidene)anabaseine (**1.45**)*

Known compound [9].

*2.1.46. 3-(6-Methoxynaphth-2-ylmethylene)anabaseine bishydrochloride(**2.1**)*

Method A, yield 69%, mp.: 223–226 °C (decomp). ^{1}H NMR (DMSO-d_6, TMS, 300 MHz, δ ppm): 9.04–8.97 (2H, m), 8.34 (1H, dt, J = 8.1, 1.8 Hz), 8.19 (1H, s), 7.99–7.83 (3H, m), 7.70 (1H, dd, J = 8.4, 1.2 Hz), 7.41 (1H, d, J = 2.7 Hz), 7.37 (1H, s), 7.25 (1H, dd, J = 9.0, 2.4 Hz), 3.91 (3H, s), 3.85 (2H, app t, J = 5.4 Hz), 3.14 (2H, app t, J = 5.7 Hz), 2.09 (2H, app quintet, J = 5.7 Hz). Anal. Calcd for $C_{22}H_{22}Cl_2N_2O$: C, 65.84; H, 5.53; N, 6.98. Found: C, 65.46; H, 5.55; N, 6.86.

*2.1.47. 3-(Benzofuran-2-ylmethylene)anabaseine bishydrochloride (**2.2**)*

Method A, yield 63%. ^{1}H NMR (DMSO-d_6, TMS, 300 MHz, δ ppm): δ 8.97 (1H, dd, J = 4.8, 1.5 Hz), 8.94 (1H, d, J = 1.5 Hz), 8.25 (1H, dt, J = 8.1, 1.8 Hz), 7.85–7.77 (2H, m), 7.73–7.66 (2H, m), 7.52 (1H, td, J = 7.2, 1.2 Hz), 7.36 (1H, td, J = 7.5, 0.6 Hz), 7.16 (1H, s), 3.85 (1H, app t, J = 5.4 Hz), 3.25 (1H, app t, J = 5.7 Hz), 2.14 (1H, app quintet, J = 5.7 Hz), contains ~5.1% of ethanol. HRMS [ESI(+)-TOF-MS] calcd for $C_{19}H_{17}N_2O$ $(M+H)^+$, Mr = 289.1335; found 289.1334.

2.2. Measurements of arylidene-anabaseine affinities for neuronal nicotinic acetylcholine receptors

Equilibrium inhibition constants (K_is) for receptor binding of the arylidene-anabaseines were measured in the Kem laboratory as

Table 1
Compound names and structures.

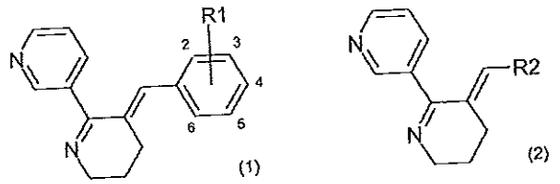

ID	Compound full IUPAC name	Substituent position
1.1	3-(4-Aminobenzylidene)anabaseine	4-NH_2
1.2	3-(4-Butoxybenzylidene)anabaseine	4-O-tC_4H_9
1.3	3-(4-Trifluoromethoxybenzylidene)anabaseine	4-OCF_3
1.4	3-(4-Methylaminobenzylidene)anabaseine	4-$NHCH_3$
1.5	3-(4-Hydroxybenzylidene)anabaseine	4-OH
1.6	3-(4-Methoxybenzylidene)anabaseine	4-OCH_3
1.7	3-(4-Methylbenzylidene)anabaseine	4-CH_3
1.8	3-(4-Methylthiobenzylidene)anabaseine	4-SCH_3
1.9	3-(4-Cyanobenzylidene)anabaseine	4-CN
1.10	3-(4-n-Propylbenzylidene)anabaseine	4-nC_3H_7
1.11	3-(4-Acetoxybenzylidene)anabaseine	4-$OCOCH_3$
1.12	3-(4-Morpholinobenzylidene)anabaseine	4-Mop
1.13	3-(4-Dimethylaminobenzylidene)anabaseine	4-$N(CH_3)_2$
1.14	3-(4-Difluoromethoxybenzylidene)anabaseine	4-$OCHF_2$
1.15	3-(4-Chlorobenzyidene)anabaseine	4-Cl
1.16	3-[4-(1H-1,2,4-Triazol-1-yl)benzylidene]anabaseine	4-Trz
1.17	3-(4-Acetamidobenzylidene)anabaseine	4-$NHCOCH_3$
1.18	3-[4-bis(2-Hydroxyethyl)aminobenzylidene]anabaseine	4-$N[(CH_2)_2OH]_2$
1.19	3-(4-Pivaloyloxybenzylidene)anabaseine	4-$OCOBut^t$
1.20	3-(4-Acetylbenzylidene)anabaseine	4-$COCH_3$
1.21	3-(4-n-Butoxybenzylidene)anabaseine	4-O-nC_4H_9
1.22	3-(2-Acetoxybenzylidene)anabaseine	2-$OCOCH_3$
1.23	3-(2-Trifluoromethoxybenzylidene)anabaseine	2-OCF_3
1.24	3-(2-Difluoromethoxybenzylidene)anabaseine	2-$OCHF_2$
1.25	3-(2-Pivaloyloxybenzylidene)anabaseine	2-$OCOBut^t$
1.26	3-(3-Methoxybenzylidene)anabaseine	3-OCH_3
1.27	3-(3-Hydroxybenzylidene)anabaseine	3-OH
1.28	3-(2,4-Dimethoxybenzyl)anabasine	2,4-$(OCH_3)_2$-Ai
1.29	3-(2-Methoxy-4-glucuronidobenzylidene)anabaseine	2-OCH_3, 4-Gluc
1.30	3-(2-i-Propoxy-4-methoxybenzylidene)anabaseine	2-OiPr, 4-OCH_3
1.31	3-[2-(Pentan-3-yloxy)-4-methoxybenzylidene]anabaseine	2-(pentan-3-yloxy), 4-OCH_3
1.32	3-(2-Acetoxy-4-methoxybenzylidene)anabaseine	2-$OCOCH_3$, 4-OCH_3
1.33	3-(2-Hydroxy-4-diethylaminobenzylidene)anabaseine	2-OH, 4-$N(C_2H_5)_2$
1.34	3-(2,6-Dimethyl-4-hydroxybenzylidene)anabaseine	2,6-$(CH_3)_2$, 4-OH
1.35	3-(3,5-Dimethyl-4-hydroxybenzylidene)anabaseine	3,5-$(CH_3)_2$, 4-OH
1.36	3-(2,4,6-Trimethylbenzylidene)anabaseine	2,4,6-$(CH_3)_3$
1.37	3-(2,4,6-Trimethoxybenzylidene)anabaseine	2,4,6-$(OCH_3)_3$
1.38	3-(3,4,5-Trimethoxybenzylidene)anabaseine	3,4,5-$(OCH_3)_3$
1.39	3-(3,4-Ethylenedioxybenzylidene)anabaseine	3,4-EDO
1.40	3-(3,4-Methylenedioxybenzylidene)anabaseine	3,4-MDO
1.41	3-(Benzylidene)anabaseine	H
1.42	3-(2,4-Dimethoxybenzylidene)anabaseine [DMXBA]	2,4-$(OCH_3)_2$
1.43	3-(2-Methoxy-4-hydroxybenzylidene)anabaseine	2-OCH_3, 4-OH
1.44	3-(2-Hydroxy-4-methoxybenzylidene)anabaseine	2-OH, 4-OCH_3
1.45	3-(2,4-Dihydroxybenzylidene)anabaseine	2,4-$(OH)_2$
2.1	3-(6-Methoxynaphth-2-ylmethylene)anabaseine	(6-CH_3O)-Nph
2.2	3-(Benzofuran-2-ylmethylene)anabaseine	2-BF

specific for either α7 ([^{125}I]α-bungarotoxin, BTX) or α4β2 ([^{3}H]cytisine) nAChRs; these were purchased from Perkin-Elmer (Boston, MA). Rat brain membranes (200 μg protein per tube) were suspended in receptor binding assay saline containing 120 mM NaCl, 5 mM KCl, 2 mM $CaCl_2$, 1 mM $MgCl_2$, 50 mM Tris Buffer (pH = 7.4) and 2 mg/ml BSA to reduce nonspecific binding [9]. Displacement of 1.0 nM BTX (~150 Ci/mmole) was measured after incubating at 37 °C for 3 h. Binding of 1.0 nM [^{3}H]cytisine (~1 Ci/mmole) was performed at 0 °C for 4 h. Nonspecific binding was measured in the presence of 1 mM nico-

filters (presoaked for 45 min in 0.5% polyethyleneimine to reduce nonspecific binding) using a Brandel Harvester; and quickly washed three times with 3.0 ml of ice-cold binding saline lacking BSA. Binding data were analyzed using GraphPad Prism™ software (San Diego, CA) [19]. The K_i values were calculated from the Cheng–Prusoff equation [20], using K_d values for each radioligand (0.32 nM for BTX, 0.92 nM for cytisine) that we determined by saturation binding analysis under identical conditions. Each reported K_i estimate is a mean value derived from three independent displacement curve determinations; the mean standard error for these

2.3. Arylidene-anabaseine pKa and Log P determinations

The pKa of the THP ring imine nitrogen was determined by analysis of the pH dependence of the arylidene-anabaseine (1.3 mM) absorbance spectrum at room temperature in the presence of 150 mM NaCl and 50 mM potassium phosphate buffer (pH = 7.4). The 250–600 nm absorbance spectrum at 13 evenly spaced pHs (range 4–10) was measured using a Beckman DU650 spectrophotometer. Absorbance values at a wavelength showing the greatest dependence on pH were then entered into the Enzfitter software [21] to calculate the pKa value. Log P, a widely used measure of lipophilicity, was determined and calculated as previously described, using the experimental pKa estimates to correct for ionization [9].

2.4. 2D-QSAR modeling

Three-dimensional conversions and pre-optimizations of the structures of all 47 compounds (Table 1) were performed using the molecular mechanics (MM+) method implemented in the HyperChem 7.5 package [22]. Final geometry optimization of the molecule was carried out by using the semi-empirical quantum-mechanical AM1 parameterization [23]. Optimized geometries of the compounds were then loaded into CODESSA PRO software [24]. Overall, more than 800 theoretical descriptors were calculated. An important stage in use of the multilinear regression QSAR is the search for the best multilinear equation among a given descriptor set. In other words, the aim is to find the best correlation of the experimental dissociation constants for binding of ligand to the nAChR (A) with a certain number, n, of molecular descriptors (D_i) weighted by the regression coefficients b_i, as defined by eq. (1):

$$A = b_0 + \sum_{i=1}^{n} b_i D_i \quad (1)$$

The Best Multilinear Regression (BMLR) method encoded in CODESSA PRO software was used to select significant descriptors for building multilinear QSAR models [25]. The treatment starts with reduction in the number of molecular descriptors. If two descriptors are highly correlated, then only one descriptor is selected (all descriptors with insignificant variance are rejected). This helps to speed up the descriptor selection and reduces the probability of including unrelated descriptors by chance.

2.5. Molecular docking

Software implementing automated docking has to deal with two conflicting requirements: i) to be based on a robust and physically relevant procedure and at the same time; ii) to keep the computational demands at a reasonable level. Two concurrent approaches for solving this conflict are currently popular: i) docking the ligands as rigid bodies (or with torsional flexibility) by scanning the protein surface for shape complementarity; and ii) building detailed energetic models employing exhaustive searches over a more limited conformational/structural space [26,27]. The AutoDock package [28] is optimized to produce reasonable results, imposing two limitations: i) no assurance of finding the global energy minima conformation of the ligand, and ii) a rigid protein target [29].

AutoGrid 4.0 [28] was used to construct a three-dimensional grid with a dimension $60 \times 60 \times 60$ Å centered at the α7 nAChR binding site. A probe atom was used to calculate the interaction energies at each grid point. Separate tables were also calculated for each atom type in the ligand, including dispersion/repulsion and hydrogen bonding energies. In addition, an electrostatic potential grid map was calculated, using a probe atom carrying a single positive charge. The electrostatic interaction energies for each ligand atom were obtained during the docking procedure as a product of the local value taken from this grid and the partial Gasteiger charge on that atom.

AutoDock 4.0 [28] was used to perform the actual docking. During the docking simulation the ligand is subjected to random rotational/translational and torsional perturbations and the interaction energy at each new position is calculated. These positions are either accepted or rejected probabilistically based on the annealing temperature of the system. The docking simulation starts at high temperature, accepting almost every move, thus allowing the ligand to explore as fully as possible the whole conformational space. With the decrease of the temperature, the unfavorable positions become increasingly disallowed. Thus, at the end of the docking procedure the ligand ultimately finds its optimal position and conformation within the deepest energetic well it has sampled. Starting from random initial states and performing multiple docking simulations, consistent favorable binding conformations could be located.

2.6. 3D-QSAR

According to the lock and key principle [30], the most active (in our case, lowest K_i) compound in the series should have

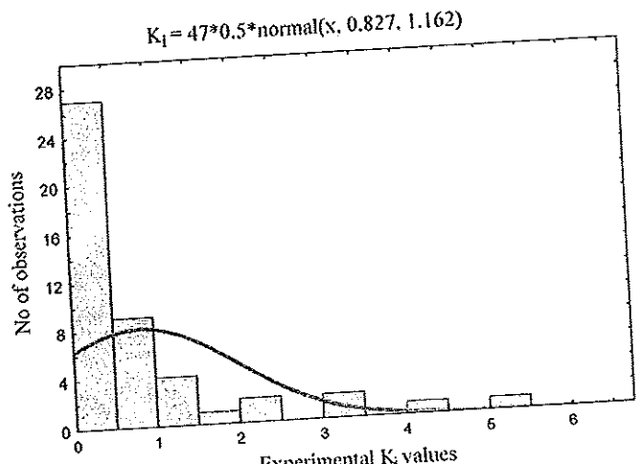

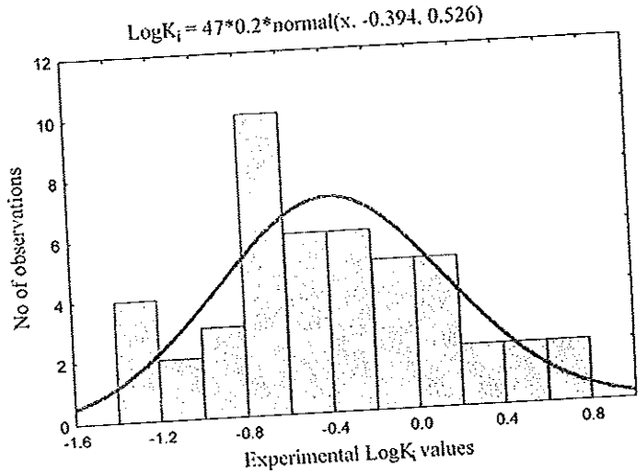

a near optimal geometry when bound to the receptor (in our case, the *Aplysia californica* AChBP). The THP-Benzylidene and THP-Pyr angles in 3-(4-Aminobenzylidene)anabaseine, the most active compound for the α7 receptor in our binding assays, were set to correspond to their most optimal values for the so-called A form of DMXBA [17] when bound to nAChBP. In accordance with the active analog approach, the so obtained geometry of 3-(4-Aminobenzylidene)anabaseine (structure 1.1, Table 1) was then used as a template for the alignment of the remaining molecules. Structure 2.1 (see Table 1) did not match the template, so it was not considered further. The flexible fitting procedure implemented in Chem-X [31] was employed to superimpose all molecules from the series (Fig. 2). Our field comparisons with flexible fitted structures are based on calculated RMS errors. Only a single conformer for each molecule was used – the one that fitted the template best.

The next step was to build a 3D grid around the set of superimposed molecules using a 1 Å grid constant. To calculate the steric and electrostatic energies of interaction a fictitious "H" probe atom with charge +1 was used. Then, the interaction energies between the probe atom and the aligned molecules were calculated for each grid point, using 0.95 cutoffs by default for both fields. When a complete probe map was calculated for each molecule in the target set, the energy values for each point in the grid were stored in columns of a study table. In the next step some or all of the grid data points can be used as descriptors in generating 3D-QSARs and analyzing structure–activity relationships.

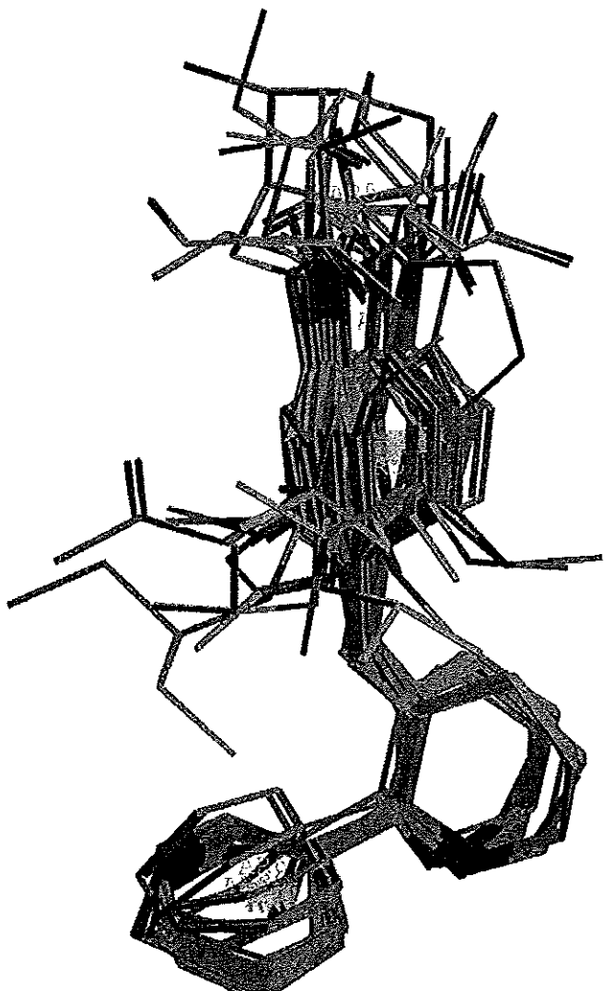

3. Results and discussion

3.1. Chemical and pharmacological diversity of the QSAR data set

A number of independent restrictions imposed by the main QSAR hypothesis sternly limits chemical diversity of the data set to the compounds that satisfy the following criteria: i) structural similarity and presence of the same pharmacophore core, ii) the same/very similar mode of action, and iii) participation in the same metabolic pathways. Therefore, the desire to construct highly accurate and statistically reliable QSAR models necessarily narrows the domain of applicability down to only 3-(arylidene) anabaseines.

The data set of the 47 arylidene-anabaseines included experimental equilibrium dissociation constants for receptor (specific) binding to rat α7 and α4β2 nAChRs, and additionally, compound ionization (pKa) and octanol–water distribution (Log P) estimates (Table 7). The receptor affinities of the compounds varied over 200-fold for the α7 receptor and 83-fold for the α4β2 subtype nAChR. Imine nitrogen basicity (pKa) values varied over 3 pH units and the Log P values varied over 2 logarithmic (base 10) units.

To improve the normal distribution of the data for the QSARs, the original K_i values obtained for both neuronal nAChRs were transformed using a logarithmic function. The Log K_is for both the α7 (Fig. 1) and α4β2 K_i values possessed distributions close to normal. The initial data set of 47 compounds was randomly split into two subsets, conditionally denoted training and test (marked with an asterisk in Table 7) subsets.

3.2. 2D-QSAR modeling

Previous studies indicated the importance of imine nitrogen group pKa for understanding of arylidene-anabaseine binding to the alpha-7 receptor [9,32] and to some extent, variations in the experimental K_is between compounds in a more limited data set [33]. For most of the compounds in the training subset, pKa (and Log P) values were experimentally determined [33]. Hence, a quantitative structure–property relationship (QSPR) modeling procedure was applied to estimate the missing values, which are shown in *italics* in Table 7. The quality of the estimation was evaluated by using an external test set of 10 compounds. Utilizing the "principle of parsimony" ("Ockham's Razor"), models with 3 descriptors were preferred as optimal (see Tables 2 and 3 and the corresponding Figs. 3 and 4).

Table 2
QSPR Log P model.

	X	ΔX	t-test	Descriptor
0	162.9	40.53	4.019	Intercept
1	−12.19	1.877	−6.493	H-donors FPSA (version 2)
2	6.314	1.693	3.729	Maximum antibonding contribution of one MO
3	−0.5627	0.1560	−3.607	Maximum e–n attraction for bond C–C

$N = 32$; $R^2 = 0.713$; $R^2_{cv} = 0.637$; $R^2_{test} = 0.593$;
$F = 23.2$; $s^2 = 0.0685$

Table 3
QSPR pKa model.

	X	ΔX	t-test	Descriptor
0	9.693	1.999	4.849	Intercept
1	0.3045	0.06057	5.027	Charged Surface Area for atom H
2	−0.4013	0.09020	−4.450	Number of O atoms
3	0.5438	0.1833	2.966	HOMO energy

$N = 34$; $R^2 = 0.757$; $R^2_{cv} = 0.680$; $R^2_{test} = 0.726$;

$F = 31.2$; $s^2 = 0.0813$

At the second stage of our study, the experimentally available Log P and pKa values, together with those estimated (using the models of Tables 2 and 3), were imported into CODESSA Pro as external descriptors. Using a training set of 36 compounds (35 for the α4β2 receptor data), models with up to 6 descriptors were generated. To identify the structural characteristics affecting the binding to both α7 and α4β2 nAChRs subtypes their corresponding Log K_i values were modeled. While none of the derived BMLR models contained either Log P or pKa as descriptors, further examination of the correlation matrix revealed a significant relationship between pKa and the "Minimum partial charge (Zefirov) for atom N" descriptor (R = −0.67) involved in the model describing the binding to the α7 nAChR.

Table 4
Best 4-parameter model for Log Ki (α7).

	X	ΔX	t-test	Descriptor
0	7.889	2.019	3.908	Intercept
1	−0.09115	0.02311	−3.944	Structural Information content (order 2)
2	79.83	20.75	3.846	Minimum partial charge (Zefirov) for atom N
3	0.03835	0.01157	3.316	Shadow plane ZX
4	47.74	16.27	2.934	Maximum nucleophilic reactivity index for atom N

$N = 36$; $R^2 = 0.665$; $R^2_{cv} = 0.557$; $R^2_{test} = 0.398$;

$F = 15.4$; $s^2 = 0.0911$

Table 5
Best 4-parameter model for Log Ki (α4β2).

	X	ΔX	t-test	Descriptor
0	−148.1	43.51	−3.405	Intercept
1	7.128	1.502	4.747	Max n–n repulsion for bond H–C
2	−14.21	4.311	−3.297	Max total interaction for bond H–C
3	0.2220	0.06814	3.258	Min atomic state energy for atom N
4	−1.162	0.3965	−2.930	LUMO + 1 energy

$N = 35$; $R^2 = 0.650$; $R^2_{cv} = 0.532$; $R^2_{test} = 0.718$;

$F = 14.0$; $s^2 = 0.0829$

Detailed analysis of the derived models (see Tables 4 and 5, and Figs. 5 and 6) indicates the importance of quantum-chemical

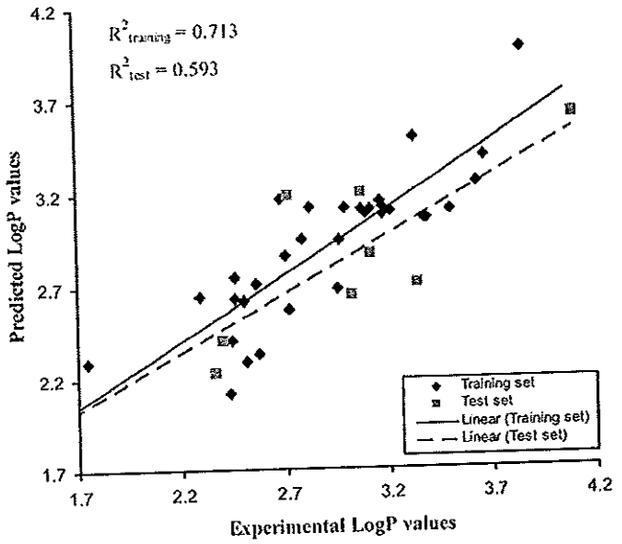

Fig. 3. Predicted vs observed Log P values.

and geometry was also revealed. Comparison of the models in Tables 4 and 5 reveals slightly different interactions governing the binding to the two nAChR subtypes. While the descriptors involved in the α4β2 model are purely electrostatic in nature, those that were most important in the case of α7 reflect also the importance of steric complimentarity for the stability of the ligand–receptor complex. This difference is consistent with a recent molecular modeling analysis of the ACh binding sites in these two receptors, based on the *Lymnaea* AChBP crystal structure, which reported that the negative electric charge of the α4β2 ACh binding site was higher than for the α7 ACh binding site [34].

In agreement with our primary goal, to understand and eventually optimize arylidene-anabaseine interaction with the α7 nAChR, this article is focused on arylidene-anabaseine binding to this rat nAChR. A 2D-QSAR model for the α4β2 subtype receptor is given for comparative purposes and for possibly providing a guide to minimizing α4β2 binding (arylidene-anabaseines generally

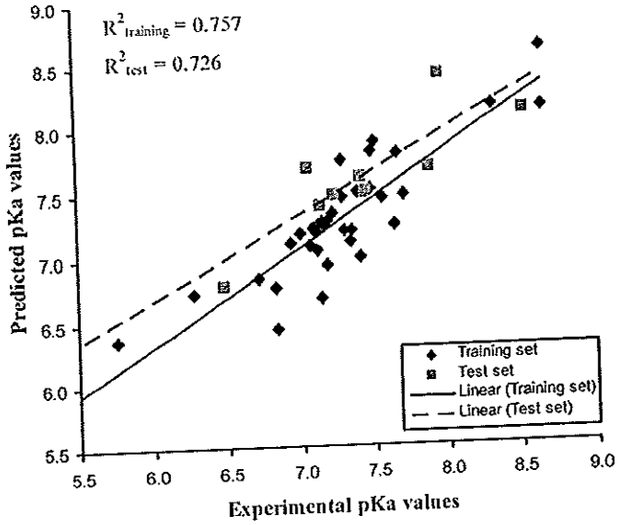

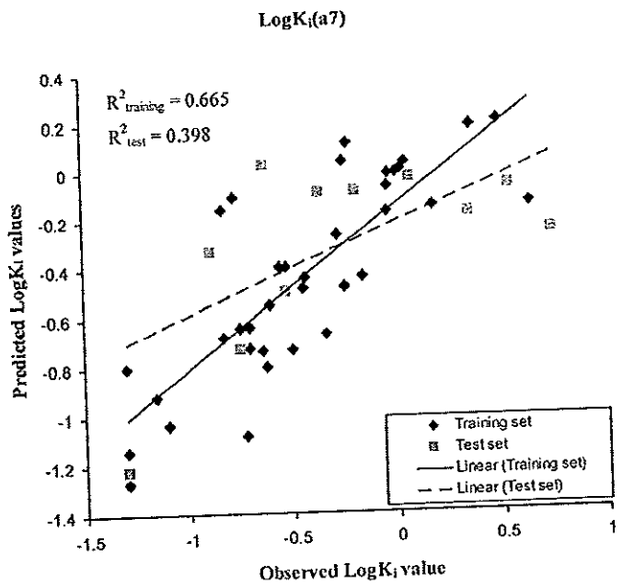

Fig. 5. Predicted vs observed α7 Log K_i values.

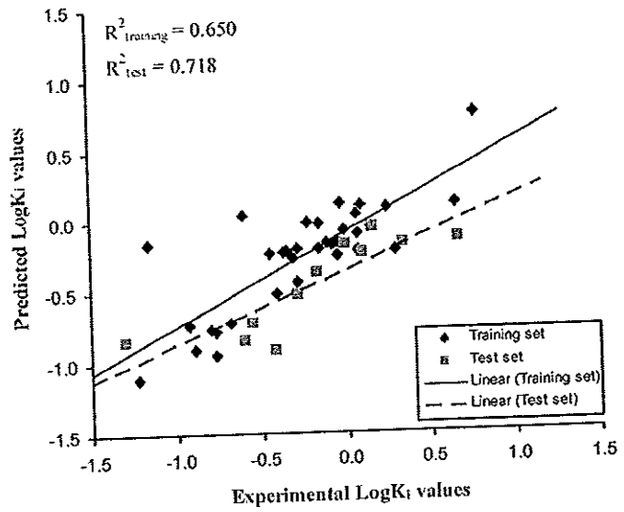

Fig. 6. Predicted vs observed α4β2 nAChR Log K_i values.

inhibit this receptor subtype; since stimulation of α4β2 receptors contributes to normal cognitive function, their inhibition would be undesirable). As already mentioned above, two of the descriptors ("Structural Information content, order 2" and "Shadow plane ZX") [25] are of topological and geometrical origin, respectively. The former depends in a complex way on the size and branching of the molecule, its flexibility and spatial mass distribution, while the latter emphasizes the significance of the orientation towards the target. The negative regression coefficient sign of the "structural information content" descriptor indicates that the increase of the molecular flexibility will result in more efficient binding to nAChR.

All ("Minimum partial charge (Zefirov) for atom N") [25] descriptor values were found to lie in the range −0.119 to −0.0987. Due to the positive regression coefficient sign of the descriptor, values in the lower range will affect the property positively. Closer examination revealed that the amino-benzylidene-anabaseines displayed some of the most negative nitrogen partial charge values, and thus were highly active. A possible explanation for their high activity could be their high propensity for formation of hydrogen bonds. The importance of the nitrogen net atomic charge was also demonstrated by Sultana et al. [35] who studied a limited data set of 9 monosubstituted anabaseines by Hansch-type approach relating pK_i (for neuronal nicotinic receptors of the cockroach, *Periplaneta americana*) to electrostatic and steric descriptors. In agreement with our conclusions it was shown that the affinity of the compounds increases as the charge of the imine nitrogen atom becomes more negative.

Table 6
Principal side amino-acids participating in π–π and H-bonding interactions.

Principal side (literature [17])	Principal side (docking)	Frequency of occurrence in percents	Complimentary side (literature [17])	Complimentary side (docking)	Frequency of occurrence in percents
Tyr93	Tyr91	75	Tyr55	Tyr53	70
Trp147	Trp145	90	Val108	Val106	35
Tyr186	Tyr186	85	Met116	Met114	35
Cys190	Cys188	70	Ile118	Ile116	80
Tyr193	Tyr193	70	Asp164	Asp162	35

According to its t-criterion, the third important descriptor is "Shadow plane ZX". It highlights the importance of the molecular size and volume, factors crucial for the insertion of the ligand into the binding pocket. The positive regression coefficient sign implies that a size over a certain threshold will hinder the access to the nAChR cleft.

The least significant descriptor in the model of Table 4 is the "Maximum nucleophilic reactivity index for atom N" [25]. It depends in a complex way on the c_i coefficients of the atomic orbitals and the HOMO energy of the molecule. Due to its complex nature, it was difficult to establish a direct relationship between certain molecular structural features accounted for by this descriptor and the experimental K_i values. Aside from any further speculations, the most unambiguous interpretation suggests the participation of donor–acceptor interactions.

Internal and external validation procedures were applied in order to estimate the predictive power of the derived models. As can be seen from Tables 4 and 5, both models are characterized by

Table 7
Experimental and calculated binding energies and K_i values.

ID	α7 (experimental K_i in μM)			K_i Docking (μM)	Binding E Docking (kCal mol^{-1})	α4β2 (experimental K_i in μM)			Log P	pKa
	K_i (μM)	Log K_i	2D-QSAR (Log K_i)			K_i (μM)	Log K_i	2D-QSAR (Log K_i)		
1.1	0.05 ± 0.003	−1.301	−1.141	0.882	−8.26	0.12 ± 0.03	−0.921	−0.731	2.43	8.33
1.2*	2.23 ± 0.48	0.348	−0.180			2.17 ± 0.24	0.336	−0.169	*3.18*	7.45
1.3	0.93 ± 0.19	−0.032	−0.015	0.960	−8.21	0.93 ± 0.09	−0.032	0.113	2.44	6.84
1.4*	0.05 ± 0.001	−1.301	−1.222	1.970	−7.78	0.05 ± 0.03	−1.301	−0.837	3.11	8.54
1.5	0.36 ± 0.02	−0.444	−0.486			0.45 ± 0.04	−0.347	−0.220	2.29	7.22
1.6	0.57 ± 0.03	−0.244	−0.480			0.49 ± 0.03	−0.310	−0.264	3.17	7.43
1.7*	0.436[a]	−0.361	−0.092	0.335	−8.83	0.99 ± 0.12	−0.004	−0.179	3.12	7.33
1.8	0.25 ± 0.003	−0.602	−0.550			0.90 ± 0.03	−0.046	−0.162	3.17	7.49
1.9	2.30 ± 0.08	0.362	0.179			1.23 ± 0.40	0.090	0.098	3.11	6.72
1.10	0.28 ± 0.02	−0.553	−0.398	0.302	−8.9	0.89 ± 0.13	−0.051	−0.249	2.82	7.39
1.11	0.17 ± 0.006	−0.770	−0.104			0.25 ± 0.01	−0.602	0.037	2.56	7.14
1.12*	0.30 ± 0.0002	−0.523	−0.497	0.811	−8.31	0.28 ± 0.09	−0.553	−0.713	2.72	7.97
1.13	0.08 ± 0.0004	−1.097	−1.034	1.170	−8.09	0.17 ± 0.005	−0.770	−0.945	3.63	8.66
1.14	1.01 ± 0.18	0.004	−0.011	3.800	−7.39	1.16 ± 0.25	0.064	0.037	3.39	7.35
1.15	1.12 ± 0.19	0.049	0.030			0.97 ± 0.38	−0.013	−0.079	3.50	7.18
1.16*	1.18 ± 0.13	0.072	−0.033	0.738	−8.37	0.52 ± 0.19	−0.284	−0.519	2.40	7.06
1.17*	0.24 ± 0.03	−0.620	0.029	1.740	−7.86	0.38 ± 0.013	−0.420	−0.911	2.36	7.42
1.18	0.19 ± 0.04	−0.721	−1.079	0.450	−8.66	0.16 ± 0.01	−0.796	−0.759	2.57	8.66
1.19	0.69 ± 0.11	−0.161	−0.441	1.120	−8.12	0.83 ± 0.25	−0.081	−0.169	3.09	7.12
1.20	0.92 ± 0.04	−0.036	−0.069	0.582	−8.51	4.49 ± 2.3	0.652	0.108	2.51	6.83
1.21	0.91 ± 0.02	−0.041	−0.172			1.96 ± 0.83	0.292	−0.215	2.68	7.67
1.22	0.57 ± 0.04	−0.244	0.039	5.210	−7.21	0.70 ± 0.36	−0.155	−0.203	2.95	6.28
1.23	3,09 ± 1.88	0.490	0.200	5.350	−7.19	1.76 ± 0.75	0.246	0.083	2.50	5.76
1.24	1.07 ± 0.04	0.029	0.000	10.450	−6.8	1.41 ± 0.01	0.149	−0.050	3.07	6.94
1.25*	0.65 ± 0.11	−0.187	−0.088	1.780	−7.84	1.44 ± 0.05	0.158	−0.057	3.34	6.48
1.26	0.46 ± 0.12	−0.337	−0.668	3.360	−7.47	1.18 ± 0.10	0.072	−0.221	3.17	7.30
1.27	0.15 ± 0.02	−0.824	−0.157			1.17 ± 0.10	0.068	−0.099	2.72	7.16
1.28	4.34 ± 0.63	0.637	−0.143			N/A	N/A	N/A	*3.43*	7.67
1.29*	0.18 ± 0.02	−0.745	−0.729			1.25 ± 0.47	0.097	−0.237	*1.97*	7.67
1.30	0.07 ± 0.03	−1.155	−0.921			0.17 ± 0.02	−0.770	−0.776	3.33	7.71
1.31	0.05 ± 0.002	−1.301	−0.801			0.43 ± 0.16	−0.367	−0.228	3.67	7.48
1.32	0.30 ± 0.09	−0.523	−0.397			0.77 ± 0.05	−0.114	−0.163	2.46	7.00
1.33	0.05 ± 0.002	−1.301	−1.272			0.13 ± 0.04	−0.886	−0.905	2.96	7.51
1.34*	5.49 ± 2.97	0.740	−0.255	1.520	−7.94	0.67 ± 0.04	−0.174	−0.370	3.02	7.14
1.35	0.53 ± 0.11	−0.276	−0.270	75.910	−5.62	0.36 ± 0.01	−0.444	−0.231	2.78	7.29
1.36	1.51 ± 0.11	0.179	−0.152			0.52 ± 0.22	−0.284	−0.437	3.12	7.19
1.37	0.18 ± 0.03	−0.745	−0.642	155.	−5.2	0.06 ± 0.03	−1.222	−1.107	3.42	7.15
1.38*	3.48 ± 2.10	0.542	−0.068	0.603	−8.48	4.67 ± 1.06	0.669	−0.142	3.07	7.23
1.39	0.20 ± 0.01	−0.699	−0.636			0.52 ± 0.01	−0.284	−0.205	3.16	7.56
1.40	0.23 ± 0.002	−0.638	−0.735			0.70 ± 0.07	−0.155	−0.027	2.99	7.64
1.41	0.60 ± 0.08	−0.222	0.114			0.85 ± 0.24	−0.071	−0.174	3.38	7.29
1.42*	0.13 ± 0.01	−0.886	−0.332			0.25 ± 0.04	−0.602	−0.839	3.86	7.11
1.43	0.24 ± 0.01	−0.620	−0.801			0.07 ± 0.030	−1.155	−0.165	3.21	7.34
1.44	0.32 ± 0.07	−0.495	−0.732			0.39 ± 0.03	−0.409	−0.511	4.10	7.89
1.45	0.20 ± 0.01	−0.699	−0.724			0.21 ± 0.016	−0.678	−0.716	2.46	7.09
2.1	0.37 ± 0.03	−0.432	−0.442	0.293	−8.91	0.60 ± 0.10	−0.222	−0.020	2.70	7.07
	0.15 ± 0.003	−0.824	−0.678			5.92 ± 1.06	0.772	0.751	1.75	7.41

[a] Values listed in *Italic* are estimated on the basis of the models shown in Tables 2 and 3.

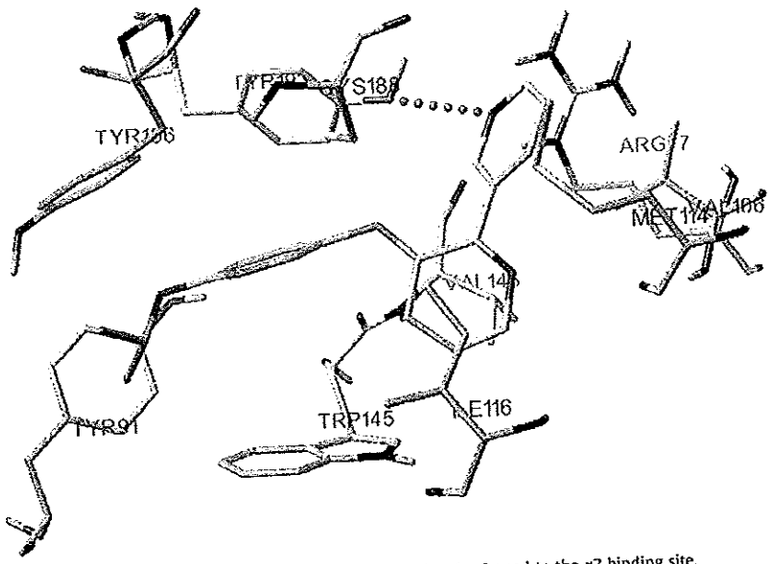

Fig. 8. 3-(4-Difluoromethoxybenzylidene)anabaseine bound to the α7 binding site.

the small differences between R^2, R^2_{CV} and R^2_{test}, which is an indication of their robustness and potential utility for predicting the binding affinities of untested compounds.

3.3. *Molecular docking*

The increased interest towards ligand binding to nAChRs resulted in significant number of molecular docking related publications during the past decade [34,36–39]. Due to the unavailability of X-ray crystallographic data of human nAChRs, different modeling AChBP systems are currently in use. Despite rather large differences in the amino acid sequences of the overall structures, sequence homology within the ligand-binding domain is relatively high. Mutations in either the nAChR or the AChBP at homologous sites within the binding sites generally produce very similar effects on ligand binding, which provides the basis for considering the AChBPs as surrogate nAChR models.

The available crystal structures of both anabaseine and DMXBA (compound **1.42**, Tables 1 and 7) when bound to the AChBP indicate that at least one water molecule mediates the binding of the ligand to the protein [17]. However, the docking procedure we used recommends the removal of the water molecules from the binding site. Thus, in our case, the screening was performed for an empty active site devoid of water. In order to achieve close agreement with the available experimental X-ray data we focused our efforts on obtaining a self-consistent picture of the intermolecular ligand–receptor interactions. Therefore, as demonstrated by Fig. 7, only those conformers that formed a domain of structures with an approximately similar axial orientation and occupied the same preferred spatial position within the ligand binding pocket were selected. The latter also happened to be the conformers with the highest binding energy. Due to the excessive computational time needed, our calculations were restricted to a subset representative of the general population. The obtained binding energies and the experimental and calculated affinity constants for binding of the ligands to the protein are listed in Table 7.

A frequency of occurrence analysis was performed in order to identify amino acid residues in the *Aplysia* AChBP which directly

AChBP (PDB identification code = 2BR7) is almost identical with the one known from the X-ray crystal structure of DMXBA and 4-OH-DMXBA bound to the same protein. Ligand interactions with both sides, principal and complimentary, of the ACh binding site were studied. The amino acid residues of the principal side involved in π–π interactions and hydrogen bonding (see Fig. 8), together with their corresponding frequencies of occurrence, are shown in Table 6. It can be seen that these derived results are in reasonable agreement with the crystallographic data for arylidene-anabaseine binding to the *Aplysia* AChBP [17] and with earlier reported docking studies. The results obtained by Huang et al. [34] using *Lymnaea stagnalis* AChBP emphasized the importance of Tyr91, Cys189 and Trp148 on the principal side; at a qualitative level these agree with our results. Similar positions were reported by Bisson et al. [37] in their docking study with *Lymnaea stagnalis* AChBP. Molecular modeling studies of binding of DMXBA and its metabolites performed on the same protein

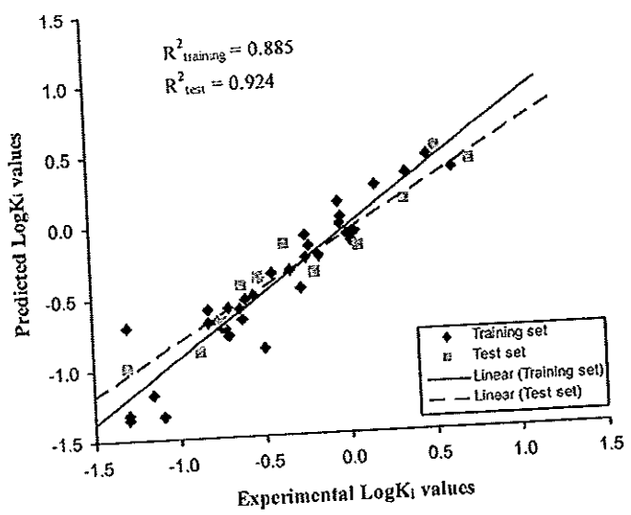

ed vs experimental Log K_i values for α7 nAChR binding for the electro-

structure revealed the significance of Tyr93, Trp149, Tyr188, Cys190 and Tyr195 [39].

Two orientations of DMXBA were observed in its crystal structure with *Aplysia* AChBP. The B orientation, being similar to that of the α7 nAChR antagonist methyllycaconitine (MLA) orientation, is thought to represent a less efficacious orientation [17]. On the other hand, the A orientation, which is also observed for the more efficacious 4-OH-DMXBA, is thought to represent the more efficacious orientation of DMXBA. The complimentary side contacts which were observed in our docking are for the most part related to the A orientation.

3.4. 3D-QSAR results

Following the procedure described in Section 2.6, the electrostatic and steric energies of interaction were studied. A two-pass-PLS method was used to obtain the 3D-QSAR model. The first step in this method calculates the principal components and the second one yields the model and its statistical parameters. For both the steric and electrostatic fields, six principal components were generated.

A separate covariance matrix was constructed from the data table. PLS determines the full eigensystem of this matrix using a singular value decomposition (SVD) method. The matrix was rewritten in a new form, and the coefficients of the transformed variables (the principal component loadings) were evaluated and used to determine the principal component scores (a set of new variables which best explain the variance in the data). The first six principle components explained 81.3% and 70.0% of the data variance for the electrostatic and steric fields, respectively.

To evaluate the external predictive power of the model, the initial data set was divided randomly into two parts (training and test subsets) having similar distribution of the receptor affinity data. In our case, the test set contains the following compounds: **1.2, 1.4, 1.7, 1.12, 1.16, 1.17, 1.25, 1.29, 1.34, 1.38** and **1.42**.

Cross-validation PLS calculations were performed to validate the models. The calculations were repeated for 10 sample sets and the results were then averaged. Each sample set was constructed from randomly selected compounds in the training subset. The size of each sample sets was specified as 10% of the total data set and each compound was omitted only once.

3.4.1. Results for the electrostatic fields

By using the calculated PC components, a PLS model for the electrostatic interactions with the following statistical parameters was obtained: $R^2 = 0.885$, $R^2_{adj} = 0.860$, $Q^2 = 0.652$, $F = 35.939$ and a std. error estimate of 0.186.

$$\text{Log } K_i = 0.078*PC1 + 0.026*PC2 + 0.033*PC3 + 0.021*PC4 + 0.018*PC5 + 0.030*PC6 - 0.397 \quad (2)$$

A chart of the predicted vs experimental Log K_i values is shown in Fig. 9. The external predictive power of this model was evaluated using the above defined test data set. The correlation coefficient of this prediction was $R^2_{ext} = 0.924$. By using the WLS (weighted least squares) [40] method, R^2 maps were generated separately for the electrostatic and steric fields. The portions of the normal coordinate space where the variation in map data values relates to activity were visualized (see Fig. 10). An R-squared map was generated by discarding those points which did not correlate with the activity, and storing the R-squared value of the correlation for each remaining point.

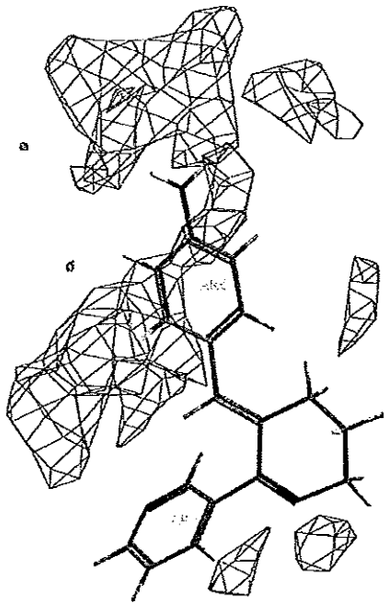

Fig. 10. WLS map of the regions important for the electrostatic fields.

following statistical parameters: $R^2 = 0.737$, $R^2_{adj} = 0.680$, $Q^2 = 0.399$, $F = 13.051$ and a std. error of estimate: 0.282:

$$\text{Log } K_i = 0.038*PC1 + 0.032*PC2 + 0.032*PC3 + 0.035*PC4 + 0.020*PC5 + 0.023*PC6 - 0.390 \quad (3)$$

A chart of the predicted vs experimental Log K_i values is shown in Fig. 11. The external predictive power of the model was again evaluated by a test series and an external predictive $R^2_{test} = 0.816$ was obtained.

Comparison of the models for the steric and electrostatic fields suggests that the electrostatic interactions play a more important role in ligand binding to the α7 nAChR. The WLS map shown in Fig. 12 indicates important regions for steric interaction in the

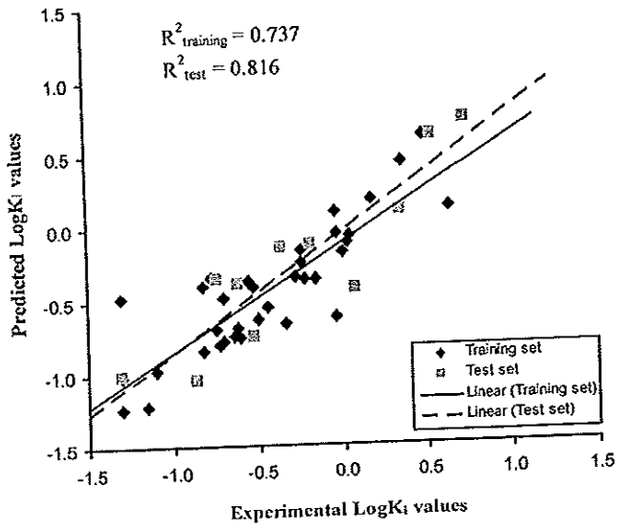

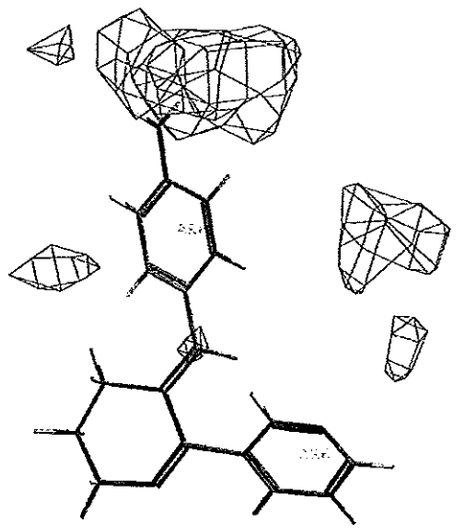

Fig. 12. WLS map of the regions important for the steric fields.

unexplored parametric space around the set of superimposed molecules.

The WLS electrostatic map (Fig. 12) identifies several regions which are important for ligand binding: positions 2 and 4 of the benzylidene moiety, and a region around the THP N atom. As can be seen in the figure, the most important regions for the steric fields are again located at positions 2 and 4 of the benzylidene moiety. Simultaneous consideration of the two maps suggests that bulky substituents at positions 2 (and due to the rotational freedom also at position 6) and 4 of the benzylidene moiety, with highly electronegative atoms at approximate distance of 3–3.5 Å projecting away from the aromatic system (at position 4) will increase binding affinity. According to the electrostatic map shown in Fig. 10, the THP N atom probably participates in a hydrogen bond with the receptor, as has been observed in previous experimental studies with DMXBA, 4-OH-DMXBA [17] and other nicotinic agonists [15,16].

4. Conclusions

Our QSAR and docking computations indicate the importance of: i) the nitrogen atom of the THP ring for hydrogen bond formation with Trp145 in *Aplysia* AChBP (and by inference, Trp147 in the α7 nAChR); ii) π–π interactions between the two aromatic rings of the ligand and the nAChBP binding site; and iii) molecular surface recognition expressed in terms of steric complimentarity. On the basis of the 3D-QSAR results, bulky substituents at positions 2 (and due to the rotational freedom also at position 6) and 4 of the benzylidene moiety, with highly electronegative atoms at approximate distance of 3–3.5 Å from the benzylidene ring (at position 4) seem optimal for enhancing the binding affinity to the α7 receptor subtype.

This initial 3-(arylidene) anabaseine QSAR analysis has focused on identifying chemical properties that determine equilibrium binding to the α7 nAChR. Future QSAR investigations will include a greater diversity of arylidene-anabaseine analogs and will focus on chemical properties that determine other important pharmacological properties in addition to receptor binding affinity, such as activation potency (EC_{50}) and apparent efficacy (maximal activation relative to maximal ACh effect).

Acknowledgments

We thank Kelly MacDougall and Renee Gallo for carrying out some of the nicotinic receptor binding experiments. The research was funded by NIH grant MH-061412 (R. Freedman and W.R. Kem).

References

[1] D.B. Kitchen, H. Decornez, J.R. Furr, J. Bajorath, Nature Rev. Drug. Discov. 3 (2004) 935–949.
[2] N. Le Novère, P.J. Corringer, J.P. Changeux, J. Neurobiol. 53 (2002) 447–456.
[3] N. Unwin, J. Mol. Biol. 346 (2005) 967–989.
[4] R. Peto, A.D. Lopez, J. Boreham, M. Thun Jr., C. Health, Lancet 339 (1992) 1268–1278.
[5] W.R. Kem, Behav. Brain. Res. 113 (2000) 169–181.
[6] L.F. Martin, W.R. Kem, R. Freedman, Psychopharmacology 174 (2004) 54–64.
[7] C.M. de Fiebre, E.M. Meyer, J.C. Henry, S.I. Muraskin, W.R. Kem, R.L. Papke, Mol. Pharmacol. 47 (1995) 164–171.
[8] W.R. Kem, V.M. Mahnir, R.L. Papke, C.J. Lingle, J. Pharmacol, Exp. Ther. 283 (1997) 979–992.
[9] W.R. Kem, V.M. Mahnir, L. Prokai, R.L. Papke, X. Cao, S. LeFrancois, K. Wildeboer, K. Prokai-Tatrai, J. Porter-Papke, F. Soti, Mol. Pharmacol. 65 (2004) 56–67.
[10] E.J. Martin, K.S. Panikar, M.A. King, M. Deyrup, B. Hunter, G. Wang, E.M. Meyer, Drug Dev. Res. 31 (1994) 134–141.
[11] G.W. Arendash, G.J. Sengstock, R. Sanberg, W.R. Kem, Brain Res. 674 (1995) 252–259.
[12] A. Olincy, J.G. Harris, L.L. Johnson, V. Pender, S. Kongs, D. Allensworth, J. Ellis, G.O. Zerbe, S. Leonard, K.E. Stevens, J.O. Stevens, L. Martin, L.E. Adler, F. Soti, W.R. Kem, R. Freedman, Arch. Gen. Psychiatry 63 (2006) 630–638.
[13] R. Freedman, A. Olincy, R.W. Buchanan, J.G. Harris, J.M. Gold, L. Johnson, D. Allensworth, A. Guzman-Bonilla, B. Clement, M.P. Ball, J. Kutnick, V. Pender, L.F. Martin, K.E. Stevens, B.D. Wagner, G.O. Zerbe, F. Soti, W.R. Kem, Am. J. Psychiat. 165 (2008) 1040–1047.
[14] K. Brejc, W.J. van Dijk, R.V. Klaassen, M. Schuurmans, J. van Der Oost, A.B. Smit, T.K. Sixma, Nature 411 (2001) 269–276.
[15] P.H. Celie, S.E. van Rossum-Fikkert, W.J. van Dijk, K. Brejc, A.B. Smit, T.K. Sixma, Neuron 41 (2004) 907–914.
[16] S.B. Hansen, T.T. Talley, Z. Radic, P. Taylor, J. Biol. Chem. 279 (2004) 24197–24202.
[17] R.E. Hibbs, G. Sulzenbacher, J. Shi, T.T. Talley, W.R. Kem, P. Taylor, P. Marchot, Y. Bourne, EMBO J. 28 (2009) 3040–3051.
[18] J.A. Zoltewicz, K. Prokai-Tatrai, L.B. Bloom, W.R. Kem, Heterocycles 35 (1993) 171–179.
[19] http://www.graphpad.com/prism/Prism.htm.
[20] Y. Cheng, W.H. Prusoff, Biochem. Pharmacol. 22 (1973) 3099–3108.
[21] http://www.biosoft.com/w/enzfitter.htm.
[22] Hyperchem, v. 7.5, Hypercube Inc., Gainesville, FL.
[23] M.J.S. Dewar, E.G. Zoebisch, E.F. Healy, J.J.P. Stewart, J. Am. Chem. Soc. 107 (1985) 3902–3909.
[24] CODESSA PRO Software. University of Florida, 2002.
[25] M. Karelson, Molecular Descriptors in QSAR/QSPR. Wiley-Interscience, New York, 2000.
[26] T.P. Lybrand, Curr. Opin. Struct. Biol. 5 (1995) 224–228.
[27] R. Rosenfeld, S. Vajda, C. DeLisi, Annu. Rev. Biophys. Biomol. Struct. 24 (1995) 677–700.
[28] M.F. Sanner, J. Mol. Graphics Mod. 17 (1999) 57–61.
[29] D.S. Goodsell, A.J. Olson, Proteins 8 (1990) 195–202.
[30] H. Kubinyi, Pharm. Acta Helv. 69 (1995) 259–269.
[31] Chem-X. Chemical Design Ltd. (now part of Accelrys), 1994.
[32] T.T. Talley, S. Yalda, K.Y. Ho, Y. Tor, F.S. Soti, W.R. Kem, P. Taylor, Biochemistry 45 (2006) 8894–8902.
[33] S.E. LeFrancois, A structure activity investigation of benzylidene anabaseine interactions with the alpha7 nicotinic acetylcholine receptor, Ph.D. dissertation, Univ. Florida, 2004, pp. 1–123.
[34] X. Huang, F. Zheng, X. Chen, P.A. Crooks, L.P. Dwoskin, C.-G. Zhan, J. Med. Chem. 49 (2006) 7661–7674.
[35] I. Sultana, I. Ideda, Y. Ozoe, Bioorg. Med. Chem. 10 (2002) 2963–2971.
[36] X. Huang, F. Zheng, C. Stokes, R.L. Papke, C.-G. Zhan, J. Med. Chem. 51 (2008) 6293–6302.
[37] W.H. Bisson, G. Westera, P.A. Schubiger, L. Scapozza, J. Mol. Model. 14 (2008) 891–899.
[38] P.H.N. Celie, S.E. Rossum-Fikkeret, W.J. Dijk, K. Brejc, A.B. Smit, T.K. Sixma, Neuron 41 (2004) 907–914.
[39] D.-Q. Wei, S. Sirois, Q.-S. Du, H.R. Arias, K.-C. Chou, Biochem. Biophys. Res. Commun. 338 (2005) 1059–1064.
[40] B. Hudson, D.J. Livingstone, E. Rahr, J. Comp-Aided Mol. Des. 3 (1989) 55–65.